Nonlinear Optics (WiSe 2018/19)
Lecture 13: January 25, 2019

12 High-harmonic generation and attoscience

12.3 Attosecond pulses

12.3.8 Attosecond ion-charge-state chronoscopy

12.3.9 Multi-purpose attoscience beamlines

Nonlinear Optics (WiSe 2018/19)
Lecture 13: January 25, 2019

in Lecture 10 already

12.3.8 Attosecond ion-charge-state chronoscopy

attosecond tunneling spectroscopy

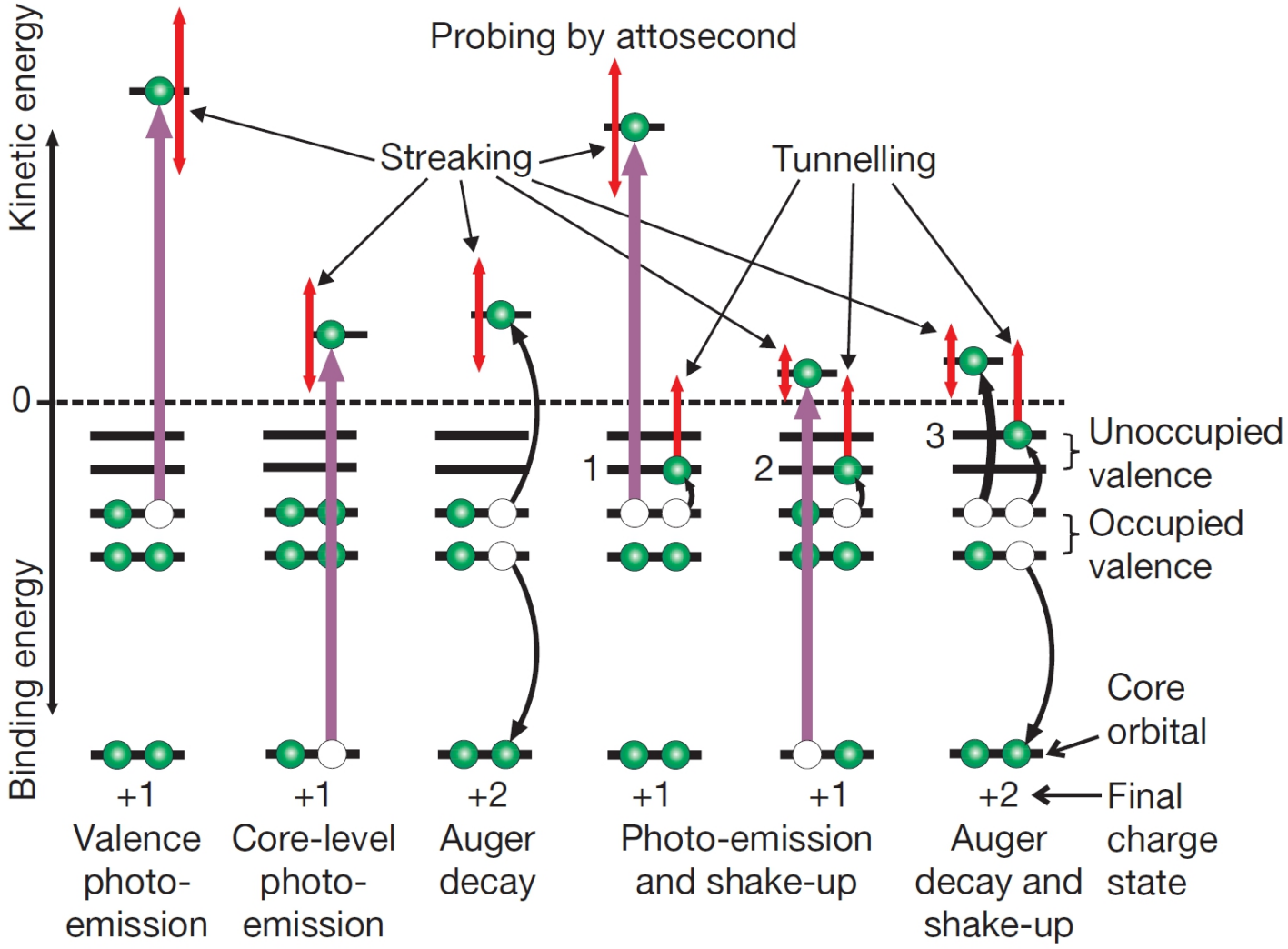

M. Uiberacker *et al.*, Nature **446**, 627 (2007)

Attosecond tunneling spectroscopy

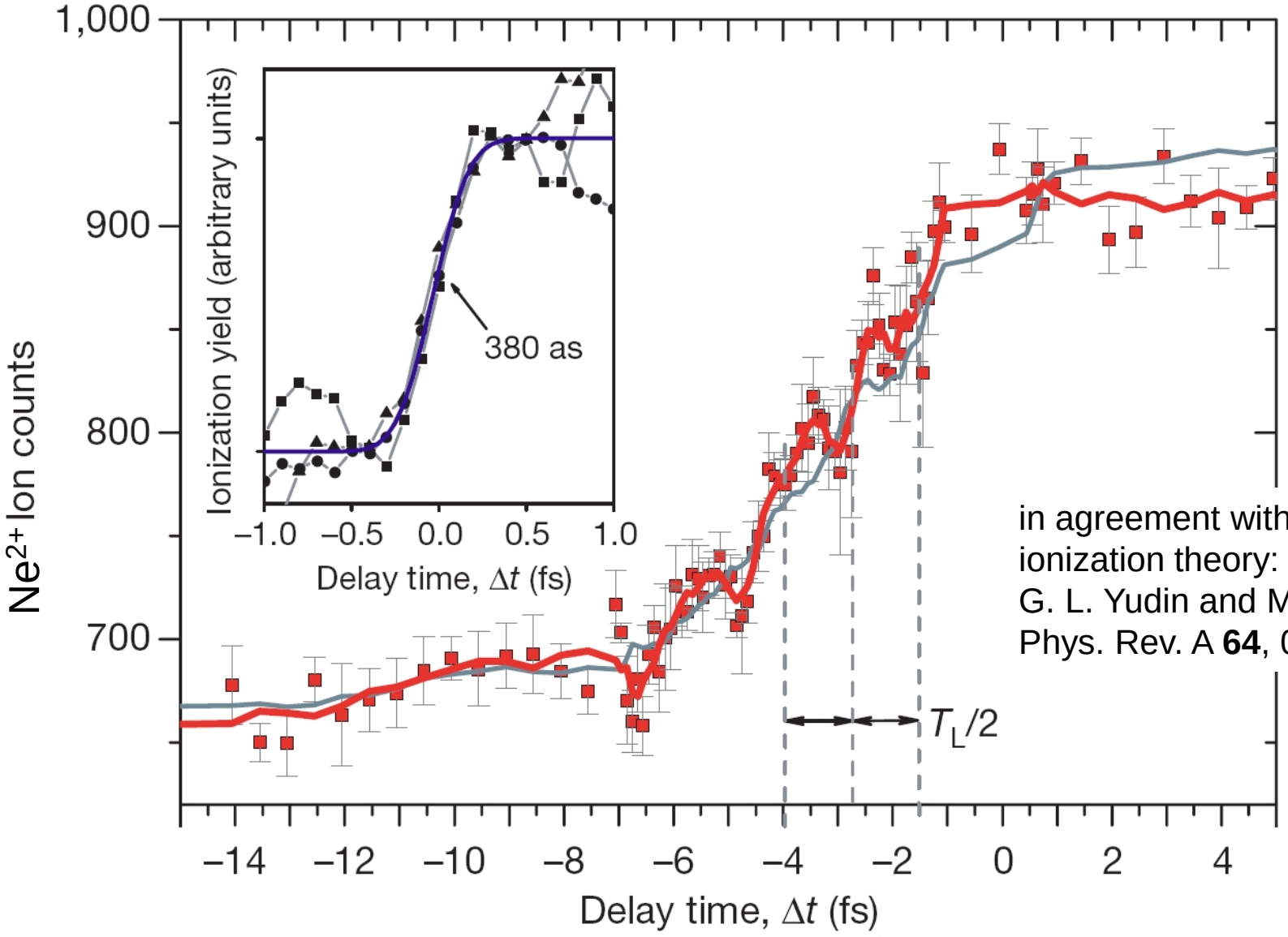

in agreement with tunnel ionization theory:
G. L. Yudin and M. Y. Ivanov, Phys. Rev. A **64**, 013409 (2001)

M. Uiberacker *et al.*, Nature **446**, 627 (2007)

Attosecond electron dynamics in amino acids

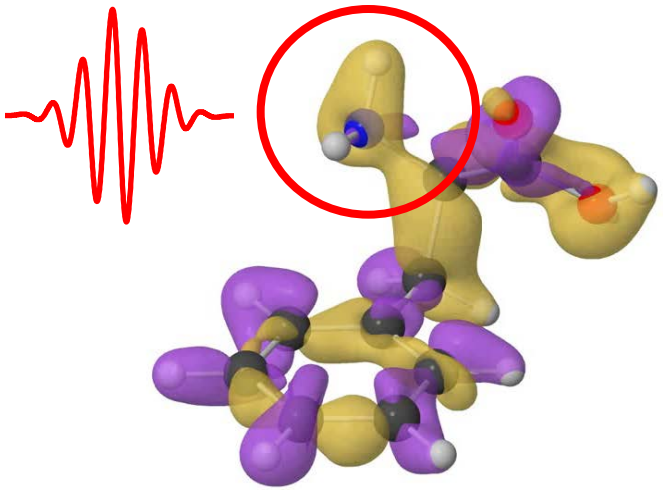

IR probe pulse is absorbed on the amino site of the molecule and it creates the doubly charged ion

fast charge density variations on the amino site produce fast yield variations in the doubly charged ion

F. Calegari *et al.*,
Science **346**, 336 (2014)

visualization of the electronic motion in real time
perspective: control of the charge localization on the electron time scale → control of the molecular reactivity on the attosecond time scale → **attochemistry**

slide courtesy of F. Calegari

12.3.9 Attoscience beamline at MPQ Garching

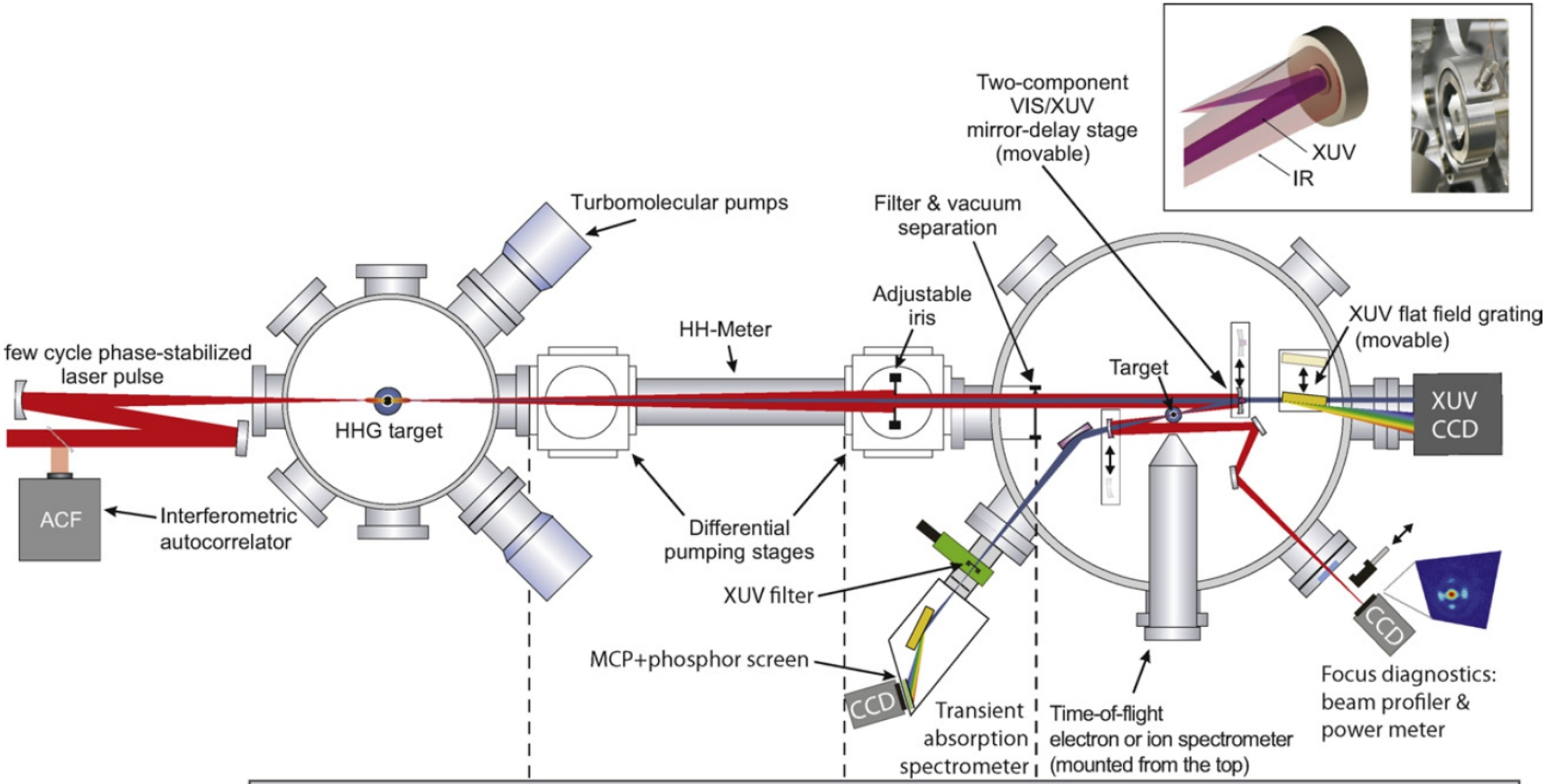

M. Schultze *et al.*, J. Electron Spectrosc. Relat. Phenom. **184**, 68 (2011)

12.3.9 Attoscience beamline at ETH Zürich

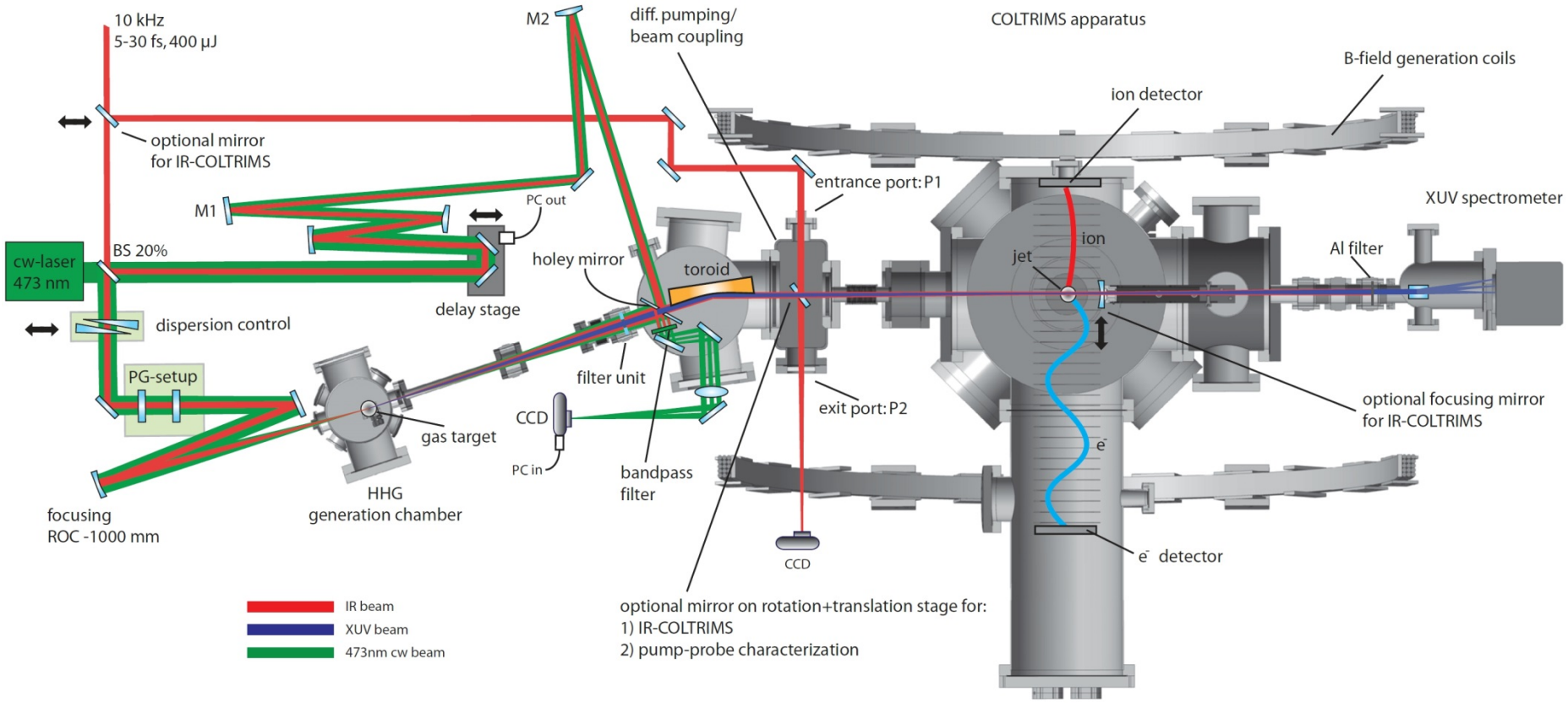

M. Sabbar *et al.*, Rev. Sci. Instrum. **85**, 103113 (2014)

Chapter 13: Strong-field physics in solids

strong-field (i.e., nonperturbative) phenomena in solids

many physical processes currently of interest in this research area already known for decades, but only thanks to the advent of modern state-of-the-art intense few-cycle pulses, in particular in mid-IR or THz, they can now experimentally be investigated

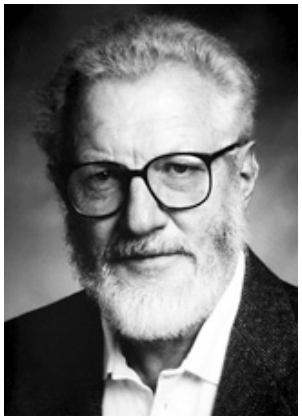

Herbert Kroemer's Nobel Prize autobiography (2000):
"… it became obvious that the huge fields required for Bloch oscillations in a **bulk** semiconductor could never be reached."

In addition, rapid progress in the field of **quantum materials**

D. N. Basov, R. D. Averitt, and D. Hsieh, Nature Materials **81**, 1077 (2017)

13.1 examples: semiconductors GaAs and ZnO

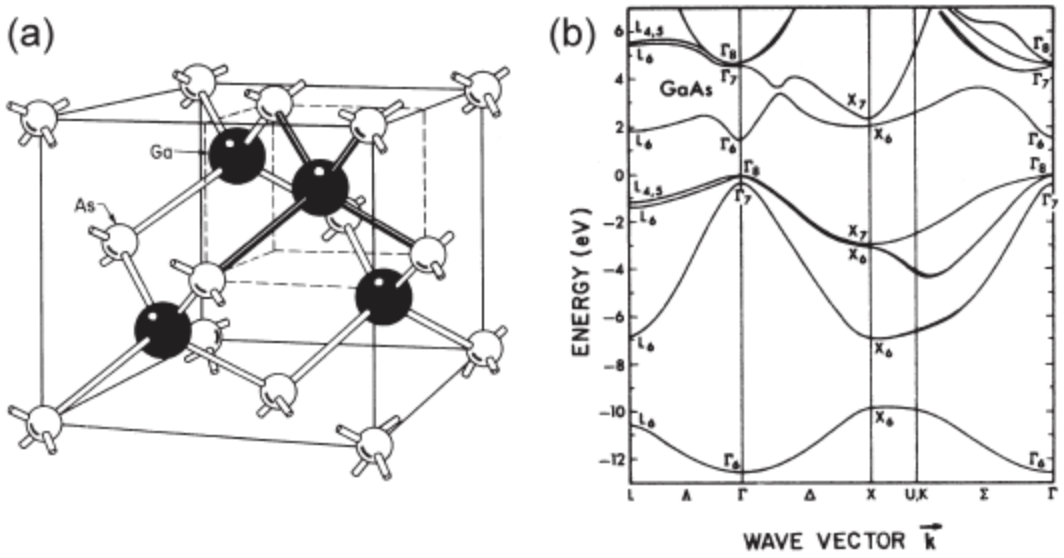

Figure 13.1: (a) Zinc blende structure of GaAs [6]. (b) Band structure of GaAs [7].

III-V direct gap semiconductor, **1.42 eV band gap**

no inversion symmetry

detailed discussion of band structure in Lecture Notes pages 308-309

13.1 examples: semiconductors GaAs and ZnO

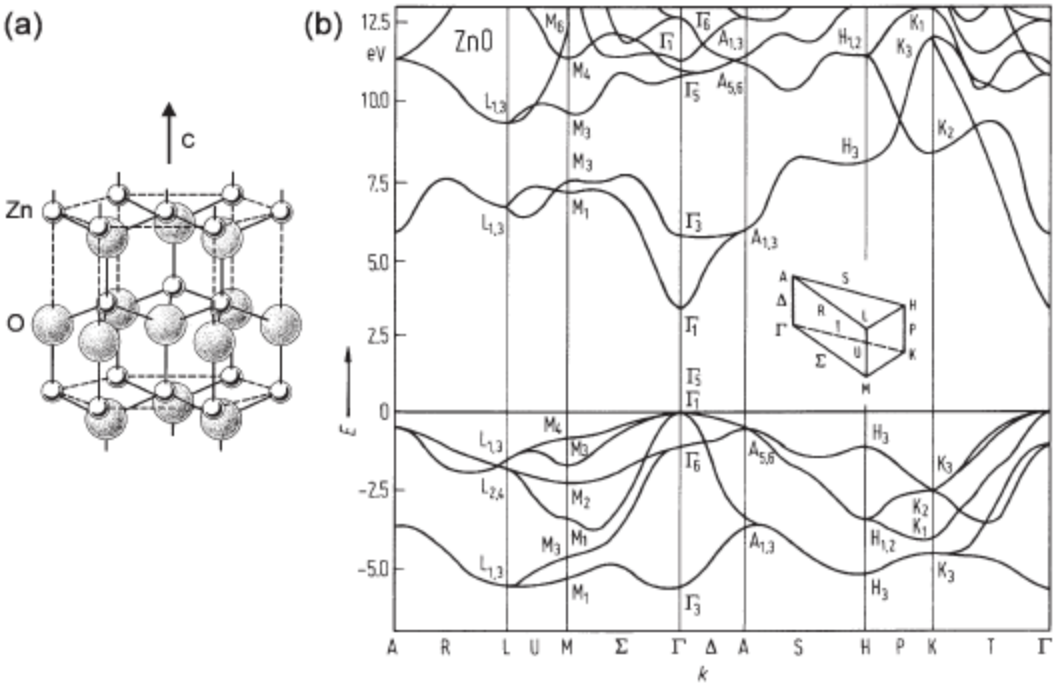

Figure 13.2: (a) Wurtzite structure of ZnO, the crystallographic $\vec{c}$-axis is indicated [9]. (b) Band structure of ZnO [10]. In this band-structure calculation, spin-orbit interaction was not included. The inset illustrates the points and directions of high symmetry of the Brillouin zone.

II-VI direct gap semiconductor, **3.3 eV band gap**

ZnO has a $\vec{c}$-axis without inversion symmetry and it is birefringent (electric field $\vec{E} \parallel \vec{c}$ and $\vec{E} \perp \vec{c}$ are inequivalent).

detailed discussion of band structure in Lecture Notes pages 309-310

Extreme nonlinear optics in solids, atoms, molecules

ponderomotive energy $U_p \propto \lambda^2 I / m_e$

semiconductors	**electron mass m_e**
resonant effects (GaAs: $\Omega/\omega_0 = 1$)	$0.067 \times m_0$
off-resonant effects (ZnO: $\Omega/\omega_0 = 2.2$)	$0.24 \times m_0$

atoms and molecules

far off-resonant effects (Neon: $I_p/\hbar\omega_0 = 14$)	m_0

$\rightarrow$ required intensities 2-3 orders of magnitude larger than in semiconductors!

strong-field excitation with UV – VIS – IR – THz driver pulses, very different from gas case which is typically far off-resonant

13.2 Energy scales of strong-field interactions in solids

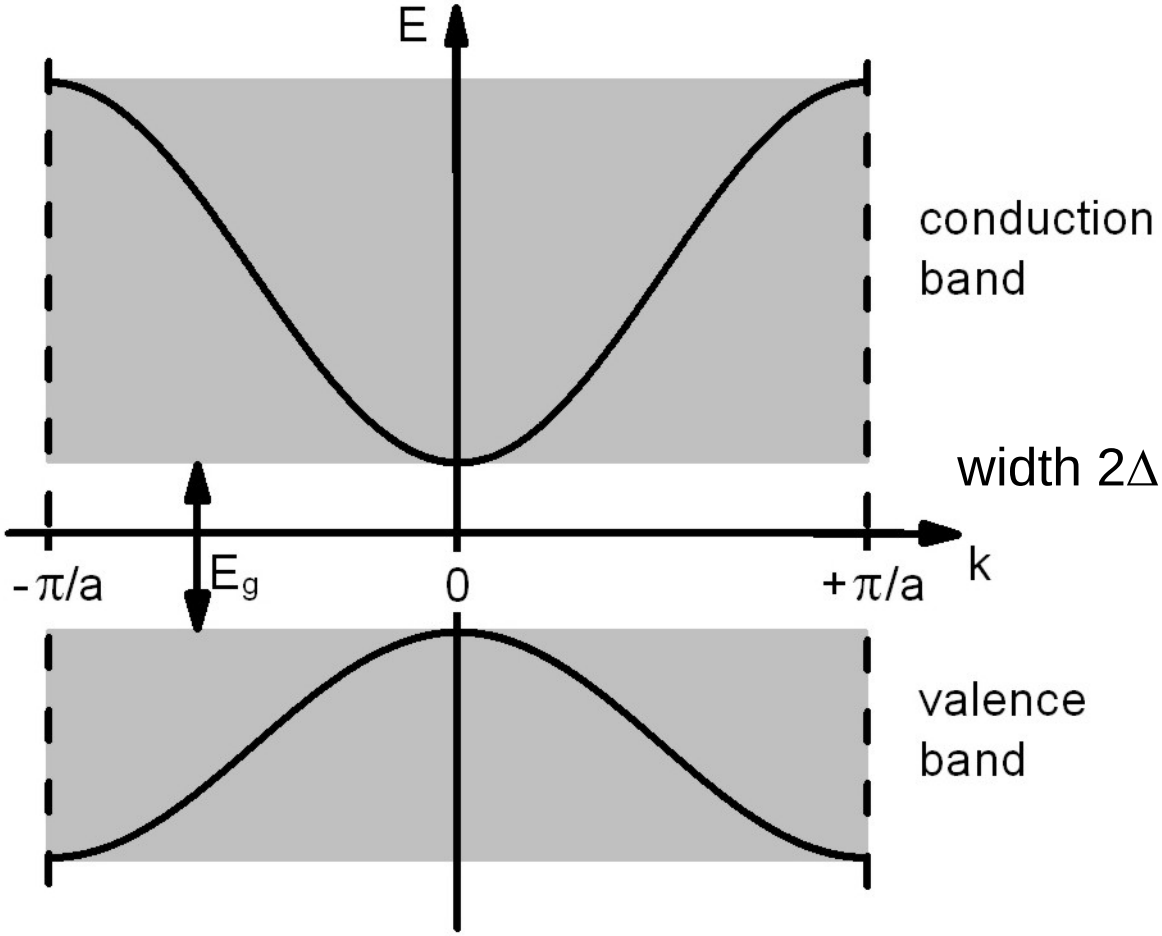

O. D. Mücke *et al.*, in Topics Appl. Phys. **95**, 379 (Springer, Berlin, 2004)

M. Wegener, *Extreme Nonlinear Optics* (Springer, Berlin, 2005)

13.2 Energy scales of strong-field interactions in solids

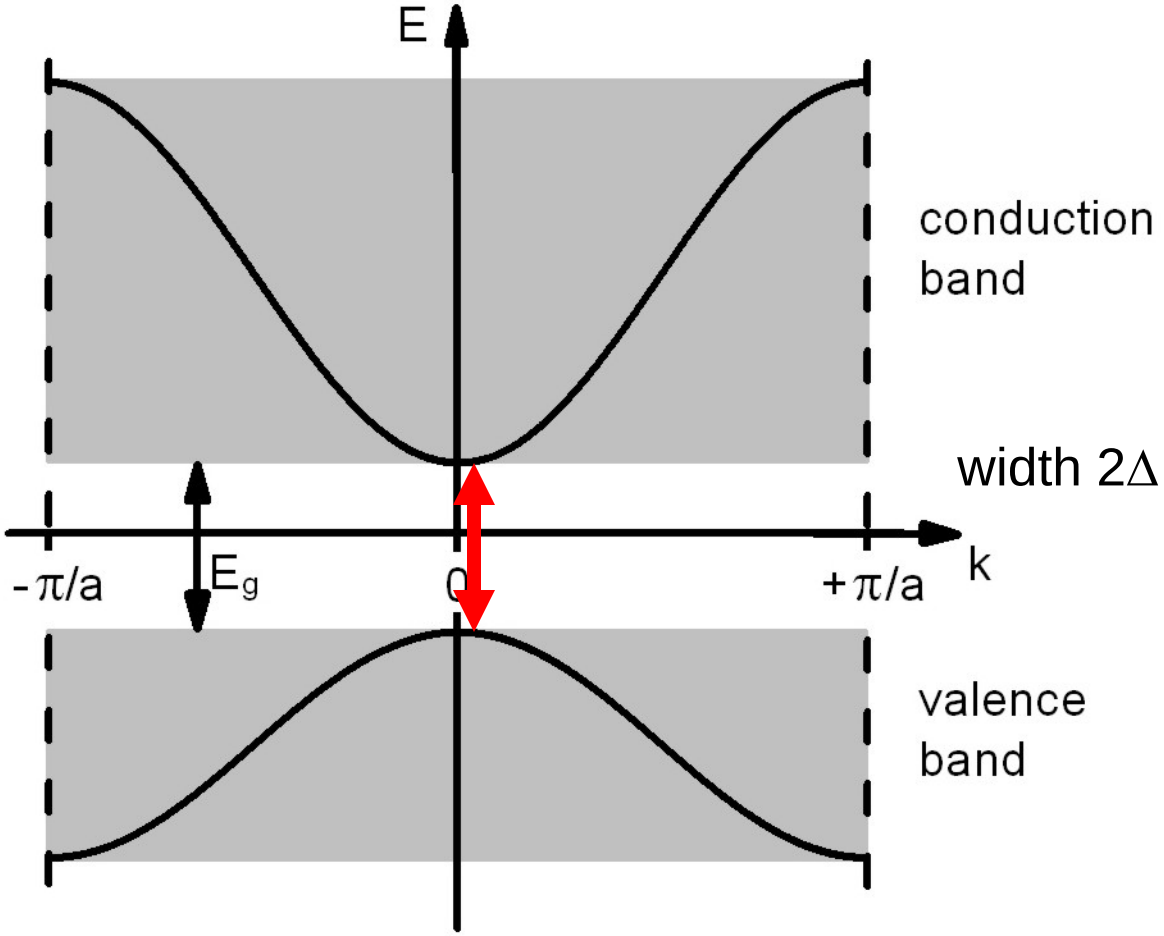

interband transitions

Rabi energy

$$\hbar\Omega_R = dE$$

optical Bloch equations

O. D. Mücke *et al.*, in Topics Appl. Phys. **95**, 379 (Springer, Berlin, 2004)

M. Wegener, *Extreme Nonlinear Optics* (Springer, Berlin, 2005)

13.2 Energy scales of strong-field interactions in solids

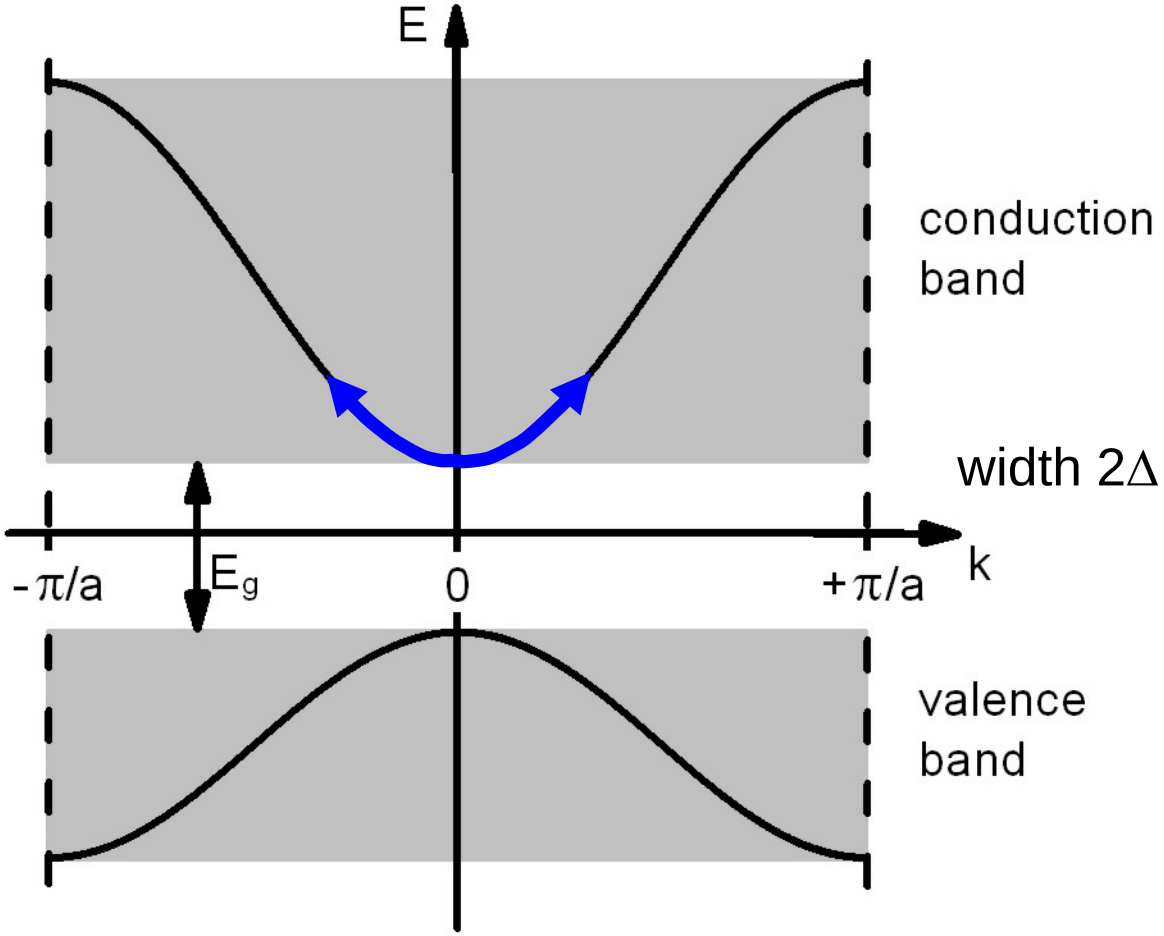

interband transitions

Rabi energy

$$\hbar\Omega_R = dE$$

intraband transitions

ponderomotive energy

$$U_p = \frac{e^2 E^2}{4 m_e \omega^2}$$

(limited validity within effective mass aproximation!)

O. D. Mücke *et al.*, in Topics Appl. Phys. **95**, 379 (Springer, Berlin, 2004)

M. Wegener, *Extreme Nonlinear Optics* (Springer, Berlin, 2005)

13.2 Energy scales of strong-field interactions in solids

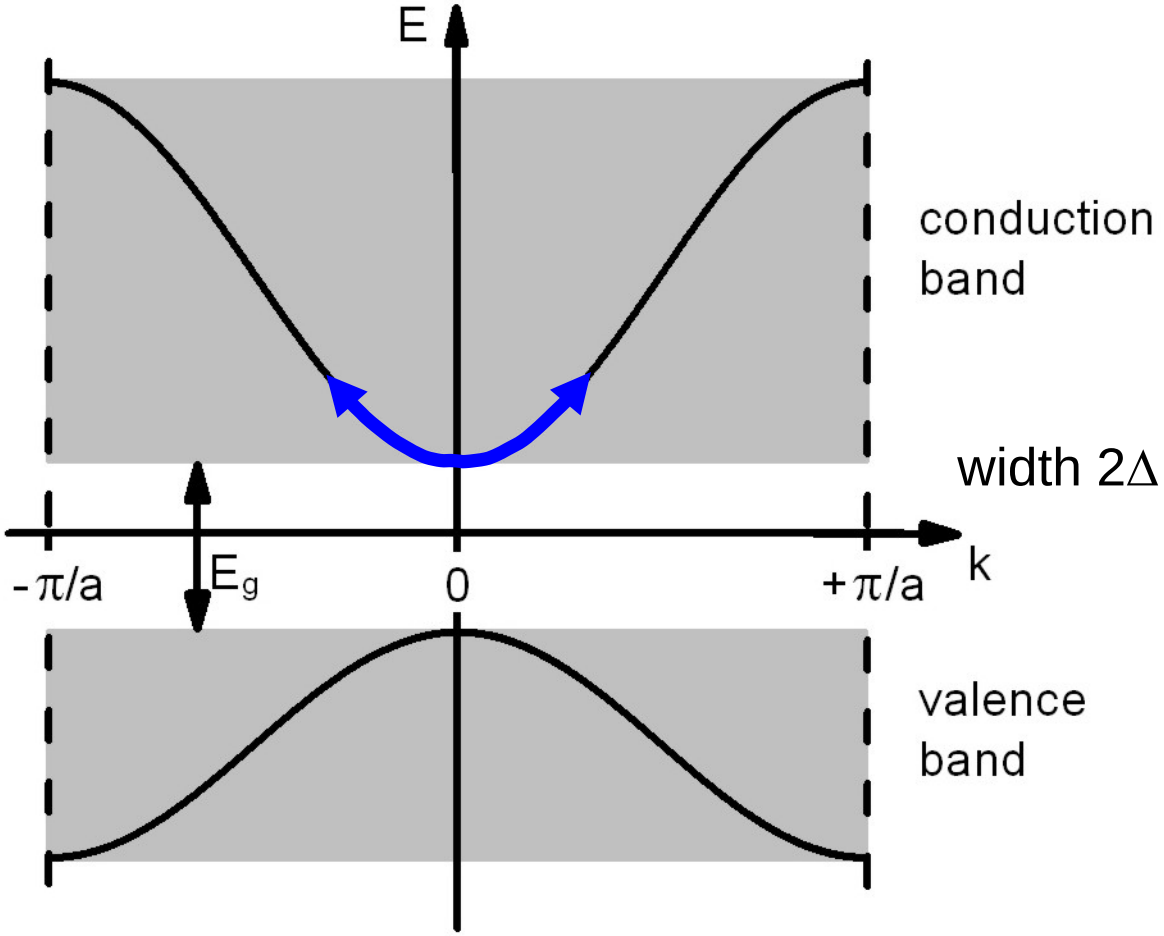

interband transitions

Rabi energy

$$\hbar\Omega_R = dE$$

intraband transitions

ponderomotive energy

$$U_p = \frac{e^2E^2}{4m_e\omega^2}$$

(limited validity within effective mass aproximation!)

Bloch energy

$$\hbar\Omega_B = aeE$$

O. D. Mücke *et al.*, in Topics Appl. Phys. **95**, 379 (Springer, Berlin, 2004)

M. Wegener, *Extreme Nonlinear Optics* (Springer, Berlin, 2005)

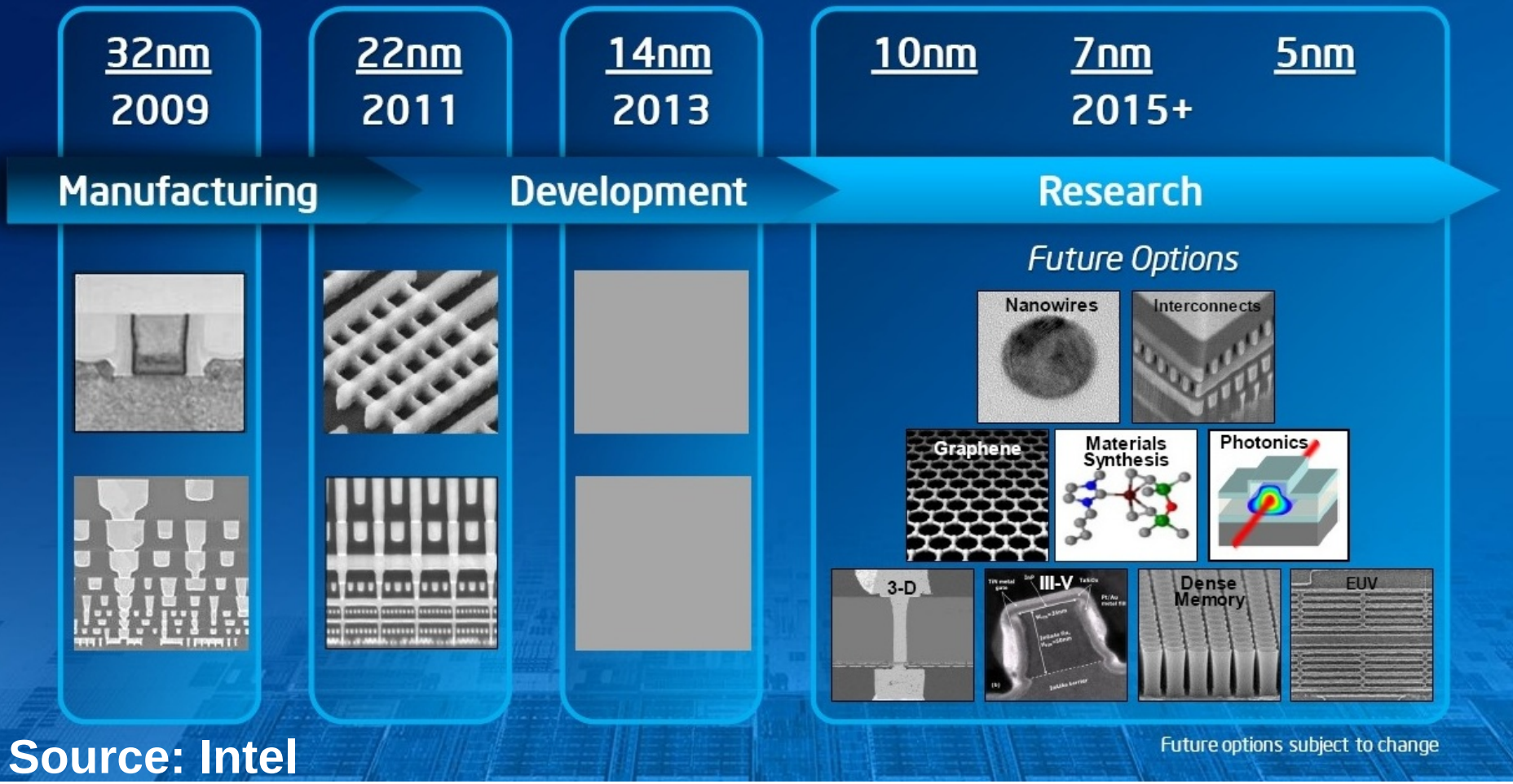

Source: Intel

ever decreasing gate length (**14nm** in 2013, potentially **5nm** in 2015+)

→ higher potential drops in semiconductor structures

→ extremely strong electric fields (~1 V/nm)

→ energy scales of strong-field interactions (ponderomotive, Rabi, Bloch energies) become comparable to characteristic energies of semiconductor (~1 eV)

extreme light-matter interactions (underlying physics, feasibility of scaling...)

13.3 Semiconductor Bloch equations

interacting **electrons and holes within a strongly excited solid** have to be treated as a **system far from equilibrium**

semiconductor Bloch equations treat the Coulomb interaction consistently on a **Hartree-Fock level**, and include many-body and phase space effects such as, **e.g., band-gap renormalization, Pauli blocking, and screening**

Hamiltonian (in second quantization, no intraband driving)

$$
\begin{aligned}
H = & \sum_{\vec{k}} E_{\mathrm{c}}(\vec{k}) c^{\dagger}_{\mathrm{c}\vec{k}} c_{\mathrm{c}\vec{k}} + \sum_{\vec{k}} E_{\mathrm{v}}(\vec{k}) c^{\dagger}_{\mathrm{v}\vec{k}} c_{\mathrm{v}\vec{k}} \\
& + \frac{1}{2} \sum_{\vec{k},\vec{k}',\vec{q}\neq 0} v(\vec{q}) \left[c^{\dagger}_{\mathrm{c},\vec{k}+\vec{q}} c^{\dagger}_{\mathrm{c},\vec{k}'-\vec{q}} c_{\mathrm{c}\vec{k}'} c_{\mathrm{c}\vec{k}} + c^{\dagger}_{\mathrm{v},\vec{k}+\vec{q}} c^{\dagger}_{\mathrm{v},\vec{k}'-\vec{q}} c_{\mathrm{v}\vec{k}'} c_{\mathrm{v}\vec{k}} + 2 c^{\dagger}_{\mathrm{c},\vec{k}+\vec{q}} c^{\dagger}_{\mathrm{v},\vec{k}'-\vec{q}} c_{\mathrm{v}\vec{k}'} c_{\mathrm{c}\vec{k}} \right] \\
& - E(\vec{r},t) \sum_{\vec{k}} \left[d_{\mathrm{cv}}(\vec{k}) c^{\dagger}_{\mathrm{c}\vec{k}} c_{\mathrm{v}\vec{k}} + \mathrm{h.c.} \right] . \qquad (13.21)
\end{aligned}
$$

The equation of motion of the optical transition amplitudes

$$p_{\mathrm{vc}}(\vec{k}) = \langle c^{\dagger}_{\mathrm{v}\vec{k}} c_{\mathrm{c}\vec{k}} \rangle \tag{13.22}$$

(depending on time t as well as parametrically on the spatial coordinate $\vec{r}$) and those of the occupation numbers in the conduction band

$$f_{\mathrm{c}}(\vec{k}) = \langle c^{\dagger}_{\mathrm{c}\vec{k}} c_{\mathrm{c}\vec{k}} \rangle \tag{13.23}$$

and in the valence band

$$f_{\mathrm{v}}(\vec{k}) = \langle c^{\dagger}_{\mathrm{v}\vec{k}} c_{\mathrm{v}\vec{k}} \rangle \tag{13.24}$$

are easily calculated from the Heisenberg equation of motion for an arbitrary operator $\mathcal{O}$ according to

$$-\mathrm{i}\hbar \frac{\partial}{\partial t} \mathcal{O} = [H, \mathcal{O}] \,, \tag{13.25}$$

while employing the usual fermionic anticommutation relations, i.e.,

$$[c_{\mathrm{c}\vec{k}}, c^{\dagger}_{\mathrm{c}\vec{k}'}]_{+} = \delta_{\vec{k}\vec{k}'} \,, \qquad [c_{\mathrm{v}\vec{k}}, c^{\dagger}_{\mathrm{v}\vec{k}'}]_{+} = \delta_{\vec{k}\vec{k}'} \,, \tag{13.26}$$

and that all other anticommutators are zero. The resulting equations of motions include couplings to higher-order correlations. With the help of a quantum-mechanical projection-operator technique it was shown in Ref. [38], that (without approximation) the density matrix can be projected into a "coherent contribution" and a "scattering contribution", respectively, and that the time evolution of an arbitrary operator $\mathcal{O}$ is governed by

$$\frac{\partial}{\partial t} \langle \mathcal{O} \rangle = \frac{\partial}{\partial t} \langle \mathcal{O} \rangle_{\mathrm{coh}} + \frac{\partial}{\partial t} \langle \mathcal{O} \rangle_{\mathrm{scat}} \,. \tag{13.27}$$

After some lengthy but straightforward operator algebra this leads to the *semiconductor Bloch equations* for the transition amplitude

$$\left(\frac{\partial}{\partial t}+\mathrm{i}\hbar^{-1}\left[\hat{E}_{\mathrm{c}}(\vec{k})-\hat{E}_{\mathrm{v}}(\vec{k})\right]\right)p_{\mathrm{vc}}(\vec{k})+\left(\frac{\partial}{\partial t}p_{\mathrm{vc}}(\vec{k})\right)_{\mathrm{scat}}=\mathrm{i}\hat{\Omega}_{\mathrm{R}}(\vec{r},\vec{k},t)\left[f_{\mathrm{v}}(\vec{k})-f_{\mathrm{c}}(\vec{k})\right], \tag{13.28}$$

for the distribution function of the conduction band

$$\frac{\partial}{\partial t}f_{\mathrm{c}}(\vec{k})+\left(\frac{\partial}{\partial t}f_{\mathrm{c}}(\vec{k})\right)_{\mathrm{scat}}=-2\mathrm{Im}\left(\hat{\Omega}_{\mathrm{R}}(\vec{r},\vec{k},t)p^{*}_{\mathrm{vc}}(\vec{k})\right), \tag{13.29}$$

and a corresponding equation for the distribution function of the valence band. The terms with subscript "scat" describe dephasing and relaxation originating from many-body interactions beyond the Hartree-Fock level. As we will see later, on a time scale close to an optical cycle, these terms can become appreciable under extreme excitation conditions.

Within the framework of the semiconductor Bloch equations, the Coulomb interaction leads to a renormalization[5] of the energies according to

$$\hat{E}_{\rm c}(\vec{k}) = E_{\rm c}(\vec{k}) - \sum_{\vec{k}'} v(\vec{k}-\vec{k}')\, f_{\rm c}(\vec{k}') \tag{13.30}$$

$$\hat{E}_{\rm v}(\vec{k}) = E_{\rm v}(\vec{k}) + \sum_{\vec{k}'} v(\vec{k}-\vec{k}')\, f_{\rm v}(\vec{k}') \tag{13.31}$$

as well as to a renormalized Rabi energy

$$\hbar\hat{\Omega}_{\rm R}(\vec{r},\vec{k},t) = d_{\rm cv}(\vec{k})E(\vec{r},t) + \sum_{\vec{k}'} v(\vec{k}-\vec{k}')p_{\rm vc}(\vec{k}')\,. \tag{13.32}$$

Thus, the carriers do not react to the applied laser field $E(\vec{r},t)$ alone, but to the applied laser field plus the "internal" field which is the sum over interband transition amplitudes $p_{\rm vc}$ times the Coulomb interaction v. Furthermore, the renormalization terms lead to a coupling of different $\vec{k}$ states.

The *optical polarization*, which enters the Maxwell equations, is given by

$$P(\vec{r},t) = \sum_{\vec{k}} d_{\rm cv}(\vec{k}) \left(p_{\rm vc}(\vec{k}) + {\rm c.c.}\right) + P_{\rm b}(\vec{r},t)\,, \tag{13.33}$$

Sometimes, a background polarization $P_{\rm b}(\vec{r},t) = \varepsilon_0\chi_{\rm b}(\vec{r})E(\vec{r},t) = \varepsilon_0(\varepsilon_{\rm b}(\vec{r}) - 1)E(\vec{r},t)$ is employed, which approximately accounts for all "very" high-energy optical transitions not explicitly accounted for in the underlying Hamiltonian. It can be expressed in terms of the background dielectric constant $\varepsilon_{\rm b}(\vec{r})$.

Now, including additional terms in the Hamiltonian (13.21), that also take into account *intraband driving*

$$H_{\rm intra} = {\rm i}eE(\vec{r},t)\sum_{\vec{k}}\left[c^{\dagger}_{{\rm c}\vec{k}}\nabla_{\vec{k}}c_{{\rm c}\vec{k}} + c^{\dagger}_{{\rm v}\vec{k}}\nabla_{\vec{k}}c_{{\rm v}\vec{k}} + {\rm h.c.}\right] \tag{13.35}$$

[but ignoring electron-phonon coupling in this section, since on time scale of the light period (i.e., the relevant scale we are interested in here in this section) electron-phonon coupling is not expected to be important (as typical phonon periods are on the order of ∼100 fs)], one can derive the *semiconductor Bloch equations for the coupled interband and intraband dynamics* [42, 43] given by

$$\begin{aligned}\left(\frac{\partial}{\partial t} + {\rm i}\hbar^{-1}\left[\hat{E}_{\rm c}(\vec{k}) - \hat{E}_{\rm v}(\vec{k})\right]\right)p_{\rm vc}(\vec{k}) + \left(\frac{\partial}{\partial t}p_{\rm vc}(\vec{k})\right)_{\rm scat}\\ = {\rm i}\hat{\Omega}_{\rm R}(\vec{r},\vec{k},t)\left[f_{\rm v}(\vec{k}) - f_{\rm c}(\vec{k})\right] + {\rm e}\hbar^{-1}E(\vec{r},t)\nabla_{\vec{k}}p_{\rm vc}(\vec{k})\,,\end{aligned} \tag{13.36}$$

and

$$\frac{\partial}{\partial t}f_{\rm c}(\vec{k}) + \left(\frac{\partial}{\partial t}f_{\rm c}(\vec{k})\right)_{\rm scat} = -2{\rm Im}\left(\hat{\Omega}_{\rm R}(\vec{r},\vec{k},t)p^{*}_{\rm vc}(\vec{k})\right) + {\rm e}\hbar^{-1}E(\vec{r},t)\nabla_{\vec{k}}f_{\rm c}(\vec{k})\,, \tag{13.37}$$

plus again a corresponding equation for the distribution function of the valence band. We immediately identify the terms related to interband transitions, $\hat{\Omega}_{\mathrm{R}}$, and to intraband transitions, $E\nabla_{\vec{k}}$. Beside the optical polarization (13.33), one has an additional source term in Maxwell's equations given by the induced *intraband current*

$$J(\vec{r},t) = \mathrm{e}\sum_{\vec{k}} \left(v_{cg}(\vec{k}) f_{\mathrm{c}}(\vec{k}) + v_{\mathrm{v}g}(\vec{k}) f_{\mathrm{v}}(\vec{k}) \right) , \tag{13.38}$$

where $\vec{v}_{ig}(\vec{k}) = \nabla_{\vec{k}} E_i(\vec{k})/\hbar$ denotes the group velocities of the valence and conduction bands ($i = \mathrm{v}, \mathrm{c}$), respectively. From the Maxwell's equation, it follows that the radiated spectrum is given by

$$I_{\mathrm{rad}}(\omega) \propto |\omega^2 P(\omega) + \mathrm{i}\omega J(\omega)|^2 \tag{13.39}$$

It is immediately clear from the semiconductor Bloch equations (13.37)-(13.37) combined with Eq. (13.39), within this theoretical framework interband and intraband transitions are inherently coupled in a nontrivial way, which generally leads to complex coupled dynamics for strong excitations, in particular for the case of high-harmonic generation from solids (see Section 13.6). Thus, it is crucial to realize, that in the general strong-field interaction case, it is *NOT possible* to experimentally isolate either interband or intraband dynamics and study them in an independent, decoupled way.

The dependence of the internal structure of a particle on the dynamical parameter can give rise to anomalous transport properties — in particular, the Berry-phase effect[174]. The Berry phase can be characterized by the Berry curvature, $\boldsymbol{\Omega}$, which behaves like an effective magnetic field in momentum space. In the context of Bloch electrons — that is, electrons that occupy a Bloch band of a crystalline solid — $\boldsymbol{\Omega}$ originates from the dependence of the periodic part of the Bloch function, $u_{n,k}$, on the wave vector $\boldsymbol{k}$. Consider a wave packet of a Bloch electron moving adiabatically in a non-degenerate energy band with band index n. In many situations, the wave packet has a real-space extension that is much larger than the lattice constant but much smaller than the length scale of the external perturbation; thus, the wave vector and the position of the wave packet can be considered simultaneously. The electron wave packet can then be described by the semiclassical transport equations of motion[14,16]:

$$\dot{\boldsymbol{r}} = \frac{1}{\hbar}\frac{\partial \boldsymbol{E}_{n,k}}{\partial \boldsymbol{k}} - \dot{\boldsymbol{k}} \times \boldsymbol{\Omega}_{n,k} \qquad \hbar\dot{\boldsymbol{k}} = -e\boldsymbol{E} - e\dot{\boldsymbol{r}} \times \boldsymbol{B}$$

where $\boldsymbol{E}_{n,k}$ and $\boldsymbol{\Omega}_{n,k}$ are the energy dispersion and Berry curvature of the nth band, $\boldsymbol{k}$ and $\boldsymbol{r}$ are the crystal momentum and position of the electron wave packet, and $\boldsymbol{E}$ and $\boldsymbol{B}$ are the external electric and magnetic field, respectively. The dot represents the first derivative with respect to time. The term $\dot{\boldsymbol{k}} \times \boldsymbol{\Omega}_{n,k}$ gives rise to an anomalous velocity perpendicular to $\boldsymbol{E}$ (that is, the Hall effect).

J. R. Schaibley *et al.*, Nature Reviews Materials **1**, 16055 (2016)

D. Xiao, M.-C. Chang, and Q. Niu, Rev. Mod. Phys. **82**, 1959 (2010)

13.6 HHG from solids
Bloch oscillations in bulk solids

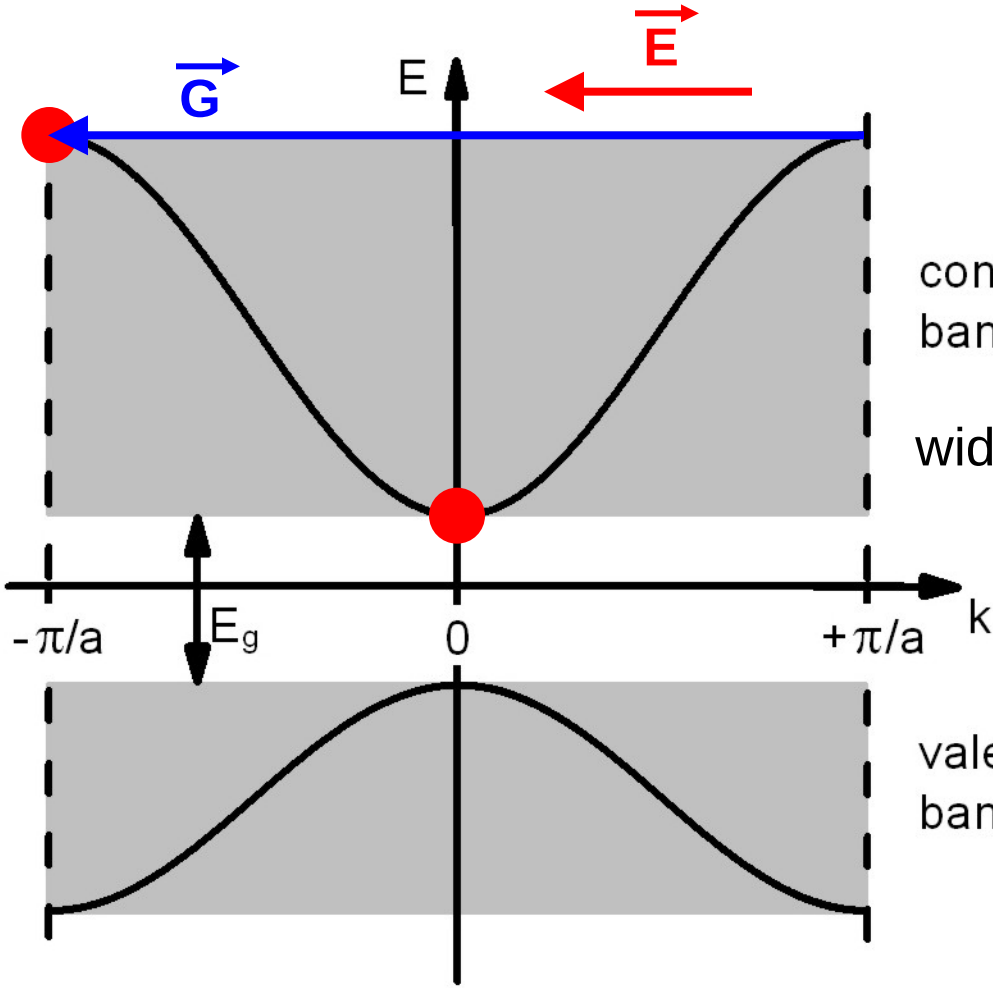

acceleration theorem

$$\vec{F} = \hbar\dot{\vec{k}} = e\vec{E}$$

Felix Bloch, Z. Phys. **52**, 555 (1929)

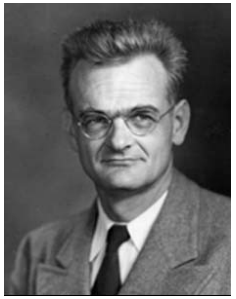

Clarence Zener, Proc. R. Soc. London A **145**, 523 (1934)

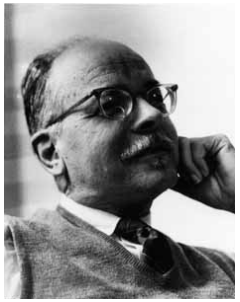

Gregory H. Wannier, Phys. Rev. **117**, 432 (1960)

Bloch oscillations in bulk solids

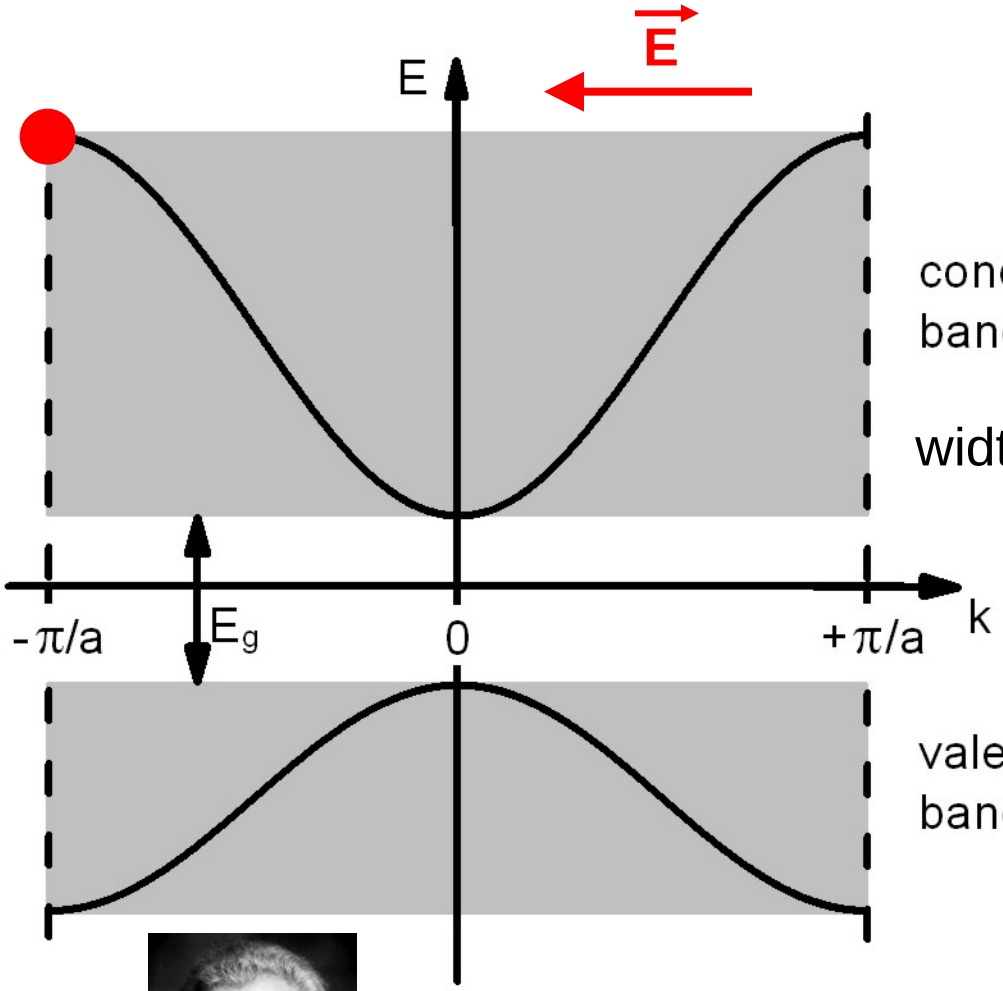

Bloch energy

$$\hbar\Omega_B = aeE$$

Bloch period

$$T_B = \frac{h}{aeE}$$

real-space oscillation diameter

$$L_B = \frac{2\Delta}{eE}$$

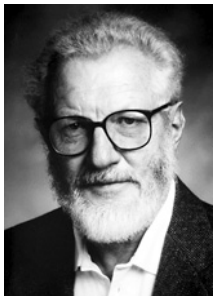

Herbert Kroemer's Nobel Prize autobiography (2000):
"… it became obvious that the huge fields required for Bloch oscillations in a **bulk** semiconductor could never be reached."

Bloch oscillations in semiconductor superlattices

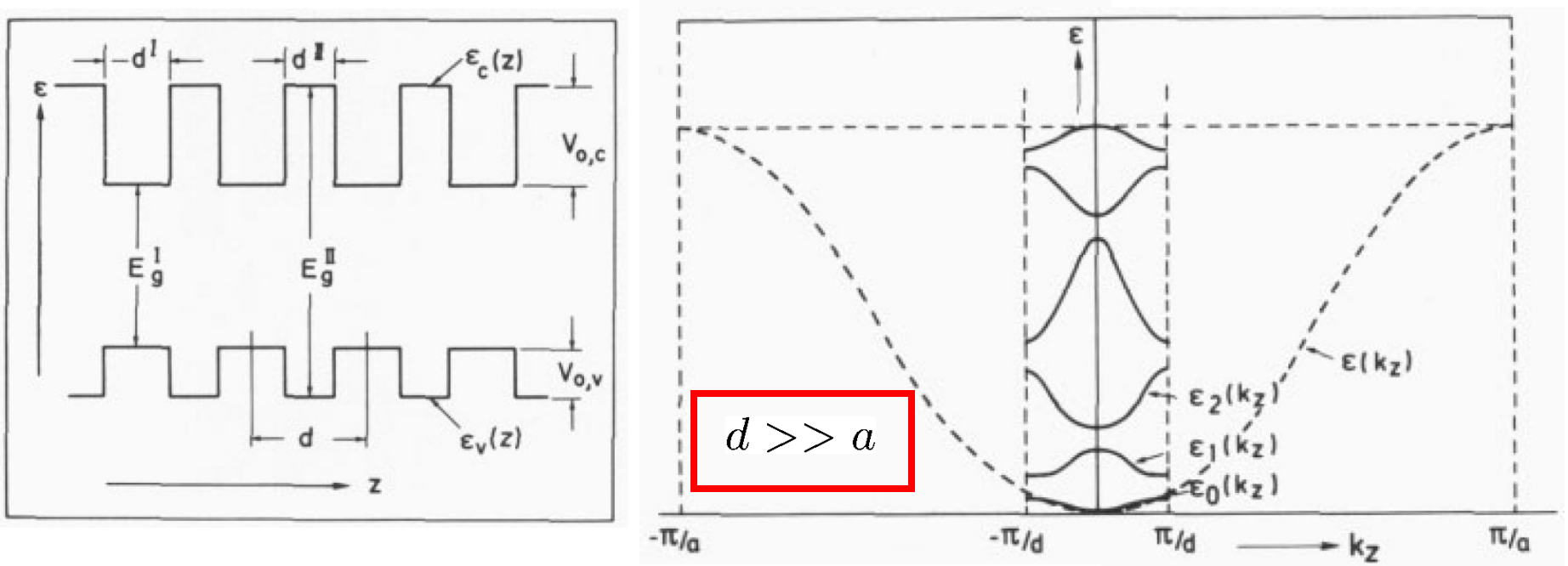

from G. H. Döhler, Physica Scripta **24**, 430 (1981)

Bloch energy $\hbar\Omega_B = deE$ Bloch period $T_B = \frac{h}{deE}$

L. Esaki *et al.*, IBM J. Res. Dev. **14**, 61 (1970):
"If the electron scattering time is sufficiently long, electrons will undergo rf oscillation due to the reflection at the minizone boundaries, the so-called “Bloch oscillation.“ "

Wannier-Stark ladders in solids

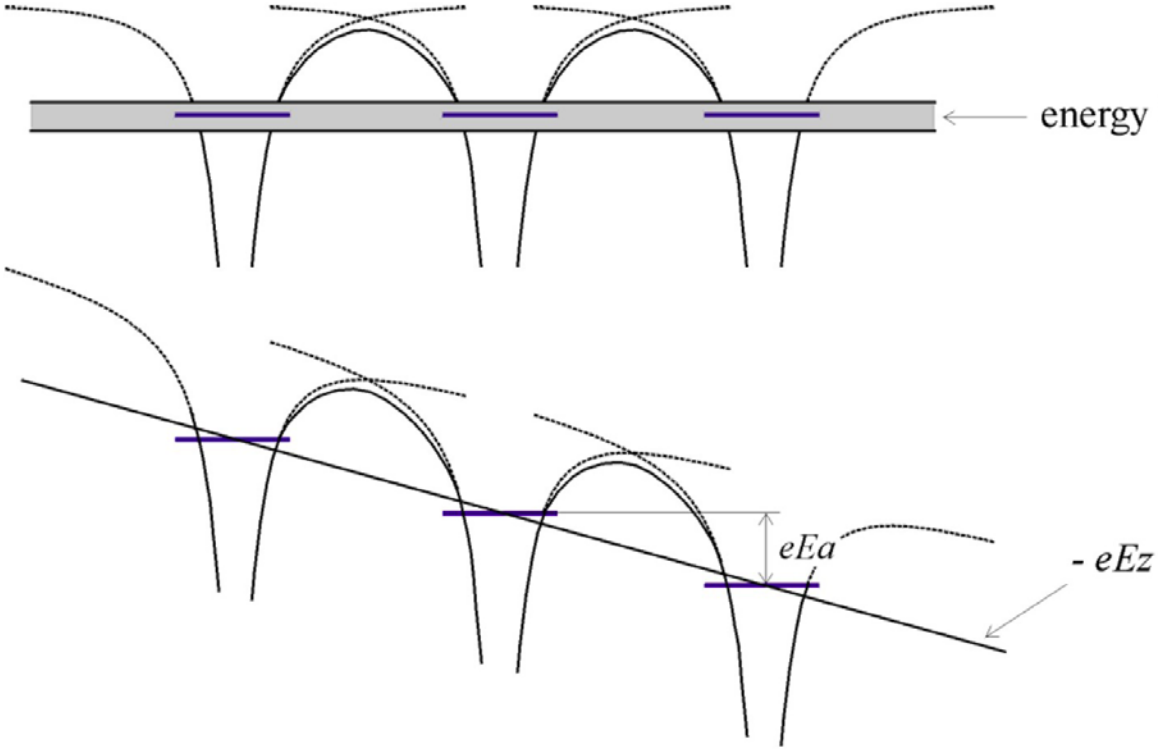

Wannier-Stark ladder

$$E_m = E_{\text{ref}} + m\,a\,\mathrm{e}\,\tilde{E}_0$$

$$m = 0, \pm 1, \pm 2, \ldots$$

electron wave packet is superposition of Wannier-Stark states, quantum beating between these states are Bloch oscillations

G. H. Wannier, “Wave Functions and Effective Hamiltonian for Bloch electrons in an Electric Field“, Phys. Rev. **117**, 432 (1960)

Equivalence of Bloch-oscillation and Wannier-Stark pictures

Hamiltonian of the system

$$\left[\frac{\left(-\mathrm{i}\hbar\nabla_{\mathbf{r}} - \frac{\mathrm{e}}{\mathrm{c}}\mathbf{A}(\mathbf{r},t)\right)^2}{2m_0} + \mathrm{e}\varphi(\mathbf{r},t) + V^{\mathrm{lat}}(\mathbf{r})\right]\phi_n(\mathbf{r}) = \epsilon_n\phi_n(\mathbf{r})$$

vector-potential gauge: $\mathbf{A}(\mathbf{r},t) = -\mathrm{c}\int_{t_0}^{t}\mathbf{E}(t')dt'$, $\varphi(\mathbf{r},t) = 0$

Bloch-oscillation picture

scalar-potential gauge: $\mathbf{A}(\mathbf{r},t) = 0$, $\varphi(\mathbf{r},t) = -\mathbf{E}(t)\cdot\mathbf{r}$

Wannier-Stark picture

total equivalence of the Bloch-oscillation and Wannier-Stark pictures, i.e., the often so-called “semiclassical Bloch picture” is on the contrary a rigorous quantum-mechanical result (Fausto Rossi, 1997)

mid-IR-driven HHG from bulk ZnO

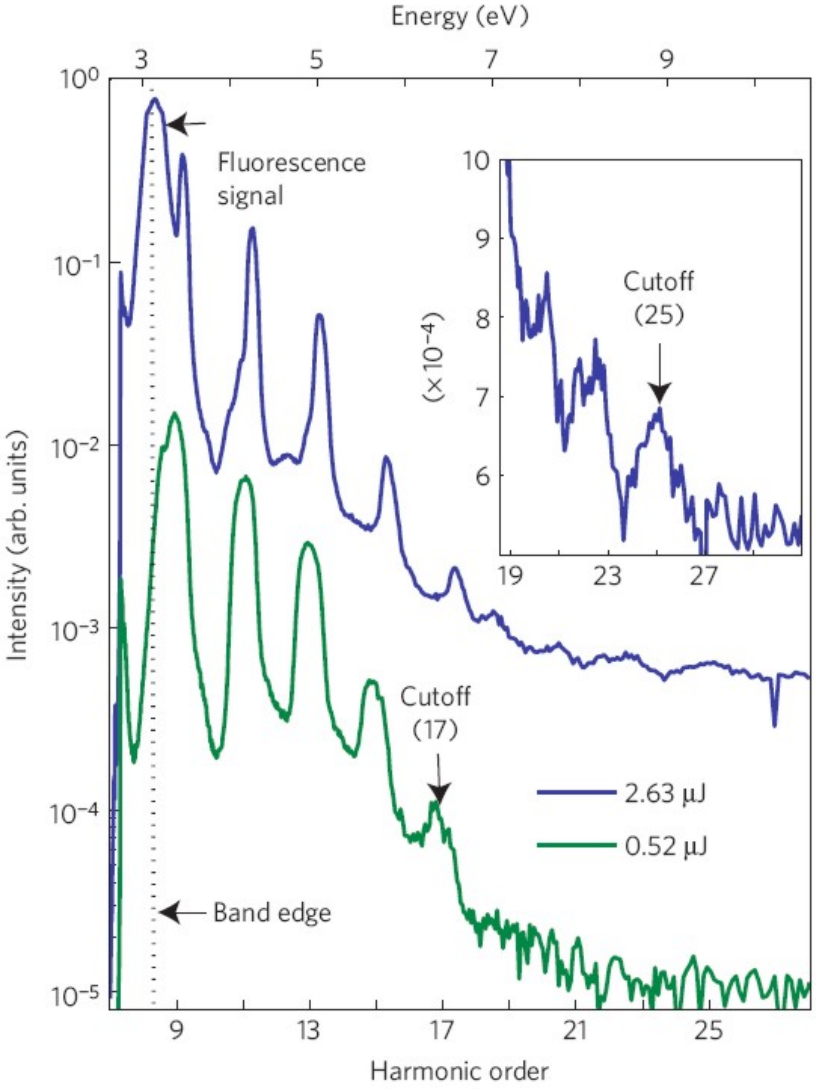

S. Ghimire *et al.*,
Nature Physics **7**, 138 (2011);
PRL **107**, 167407 (2011)
PRA 107, 167407 (2012)

500-μm-thin ZnO crystal

9-cycle-long MIR pulses (~100-fs 3.25-μm 0.38-eV pulses with up to 2.63 μJ energy, yielding a focused field strength of 6 V/nm)

Bloch HHG up to 25th order extending to >9.5 eV

J. P. Marangos, Nature Physics **7**, 97 (2011)]: "An important question not yet addressed is whether the harmonic emission retains a subfemtosecond character; that is, is it confined only to certain moments within the optical cycle? The observed bandwidth of the emission (~9 eV) is sufficient to support subfemtosecond pulses."

Bloch oscillation of an electron

"acceleration theorem": $\hbar \frac{\mathrm{d}}{\mathrm{d}t} k = -\mathrm{e}E$

time-dependent field: $a \frac{\mathrm{d}}{\mathrm{d}t} k(t) = -\Omega_{\mathrm{B}}(t)$

instantaneous Bloch energy: $\hbar \Omega_{\mathrm{B}}(t) = a\mathrm{e}E(t)$

solution: $k(t) = k_0 + \mathrm{e}A(t)/\hbar$ with $A(t) = -\int_{-\infty}^{t} \mathrm{d}t' E(t')$

k-space dynamics directly reproduces *A*(*t*), however, folded into the first Brillouin zone via Bragg reflections at the Brillouin zone boundaries

HHG from Bloch oscillating electron wave packets

tight-binding band structure: $\hbar\omega_{\mathrm{e}}(k) = \frac{\hbar^2}{m_{\mathrm{e}}a^2}\left[1-\cos\left(ka\right)\right]$

Boltzmann equation (scattering ignored): $\frac{\partial}{\partial t}f(k,t) = -\frac{\mathrm{e}}{\hbar}E(t)\frac{\partial}{\partial k}f(k,t)$

group velocity: $v_{\mathrm{g}}(k) = \frac{\mathrm{d}}{\mathrm{d}k}\omega_{\mathrm{e}}(k)$

resulting current: $j(t) \propto \mathrm{e}\int_{\mathrm{BZ}} \mathrm{d}k\; v_{\mathrm{g}}(k) f(k,t)$

source term $\partial j(t)/\partial t$ $\rightarrow$ Bloch-HHG spectrum $I_{\mathrm{rad}}(\omega) \propto \left|\omega j(\omega)\right|^2$

M. W. Feise *et al.*, Appl. Phys. Lett. **75**, 3536 (1999)

M. Wegener, *Extreme Nonlinear Optics* (Springer, Berlin, 2005)

O. D. Mücke, PRB **84**, 081202(R) (2011)

Bloch oscillating electron wave packet

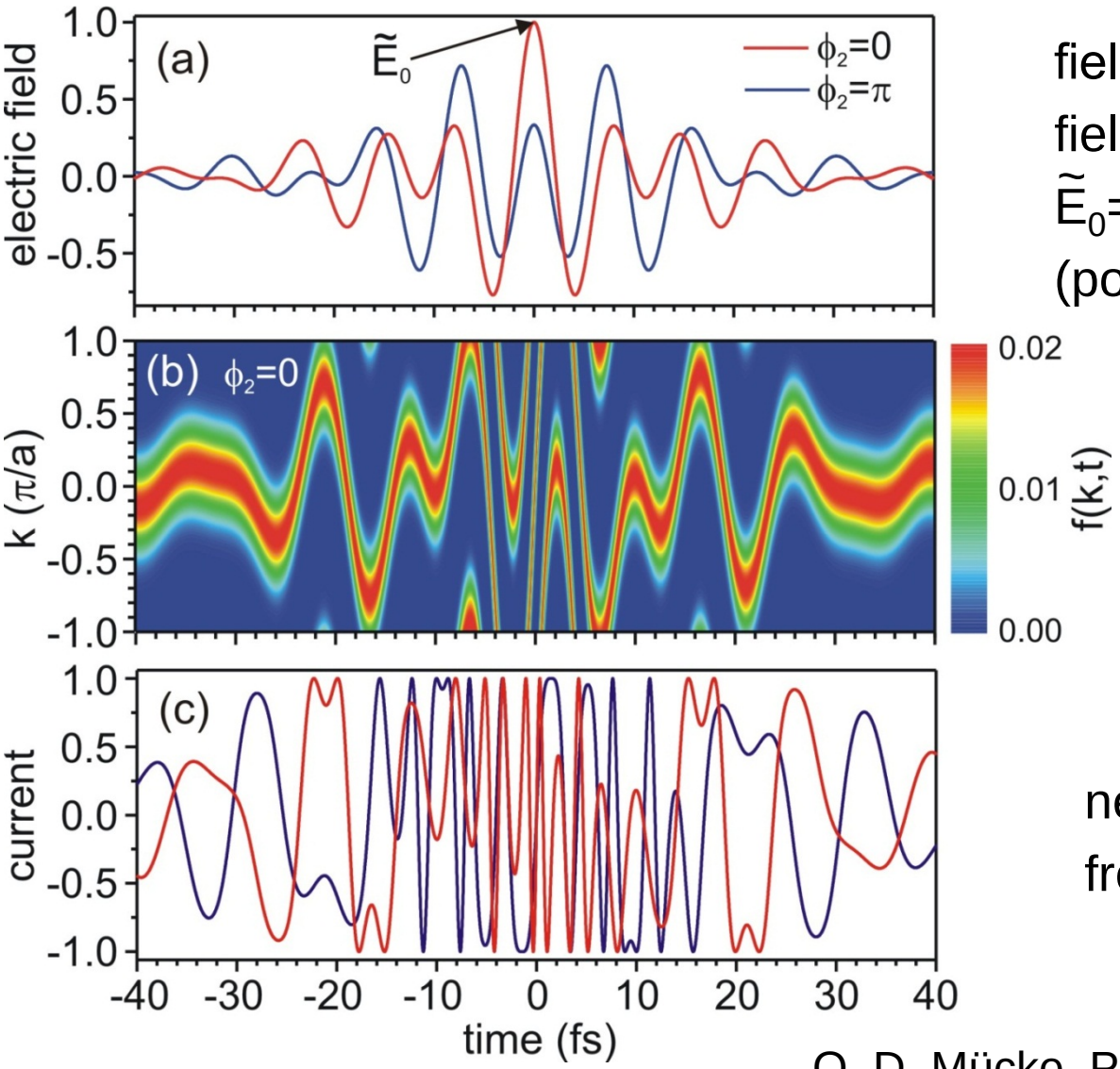

field 1: (17 fs, 2.3 μm),

field 2: (r_2 = 0.5, 25 fs, 3.6 μm)

$\tilde{E}_0$= 6.2 V/nm

(potential drop of 3V over a)

$$k(t) = k_0 + eA(t)/\hbar$$

near t=0fs, current changes from -1 to +1 within 640 as

O. D. Mücke, PRB **84**, 081202(R) (2011)

S. Ghimire *et al.*, Nature Physics **7**, 138 (2011)

O. D. Mücke *et al.*, Opt. Lett. **27**, 2127 (2002)

Time-frequency analysis using Gabor transform

$$H(\omega,t)=\left|FT_{t'}\left\{\frac{\partial j(t')}{\partial t}e^{-(t-t')^2/T_G^2}\right\}\right|^2$$

T_G=0.7 fs

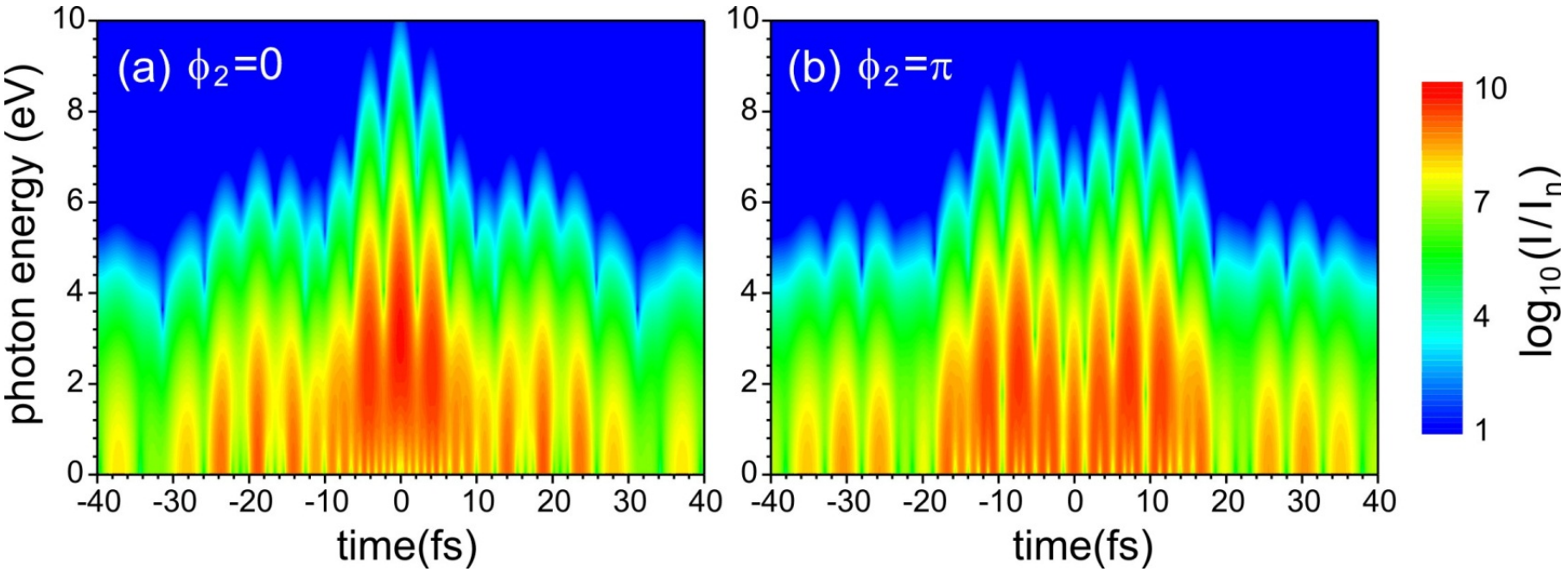

lower harmonic orders: emitted at several instants during one optical cycle

highest harmonic orders: emitted only during extrema of electric field

Important: It is obviously NOT feasible to compress the total ~9 eV bandwidth to an isolated attosecond pulse because of the complicated chirp

Cutoff filtering of Bloch-HHG

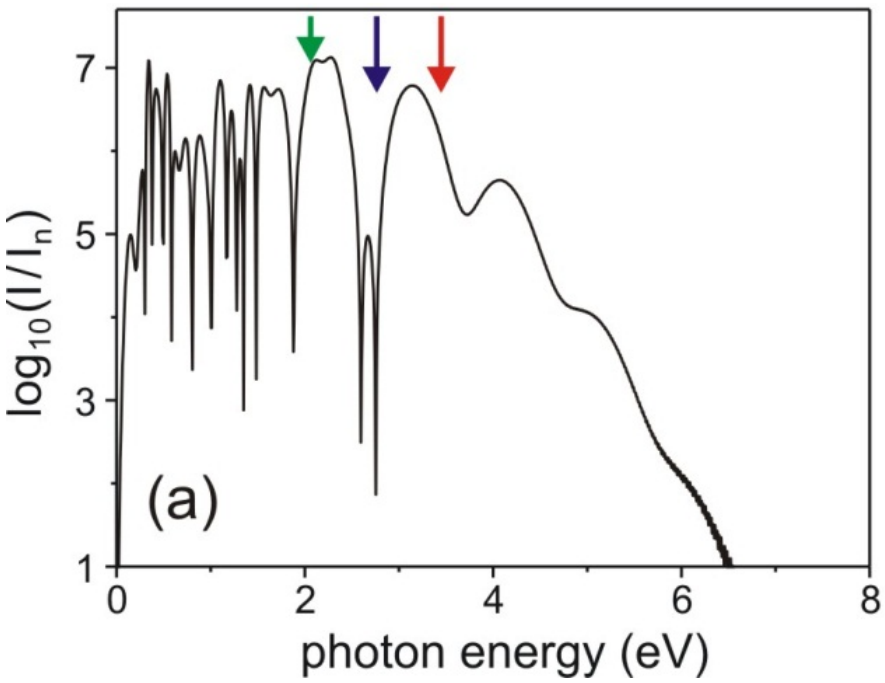

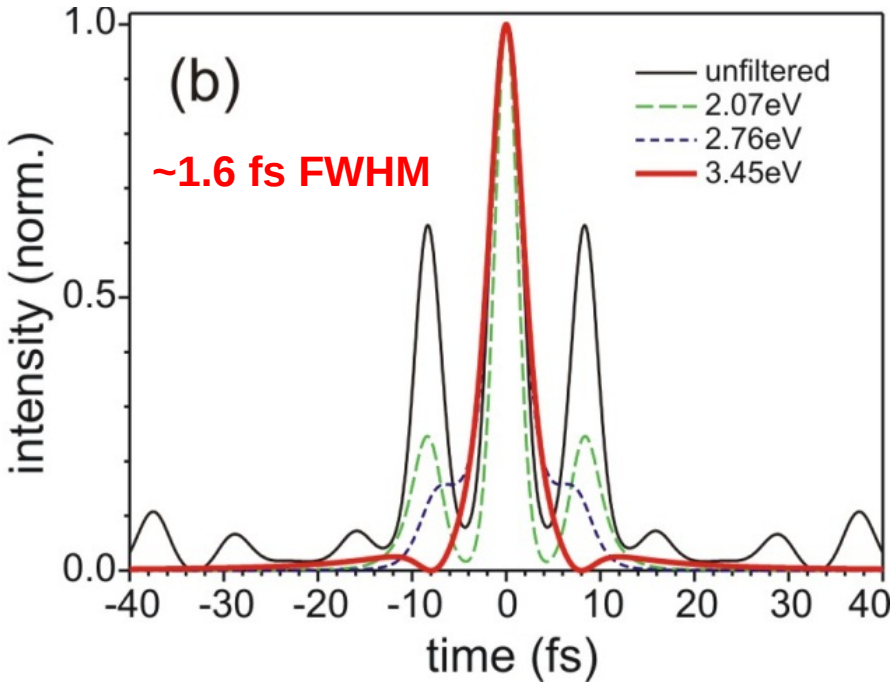

isolated Bloch-HHG pulse of ~1.6-fs FWHM duration

Influence of band structure

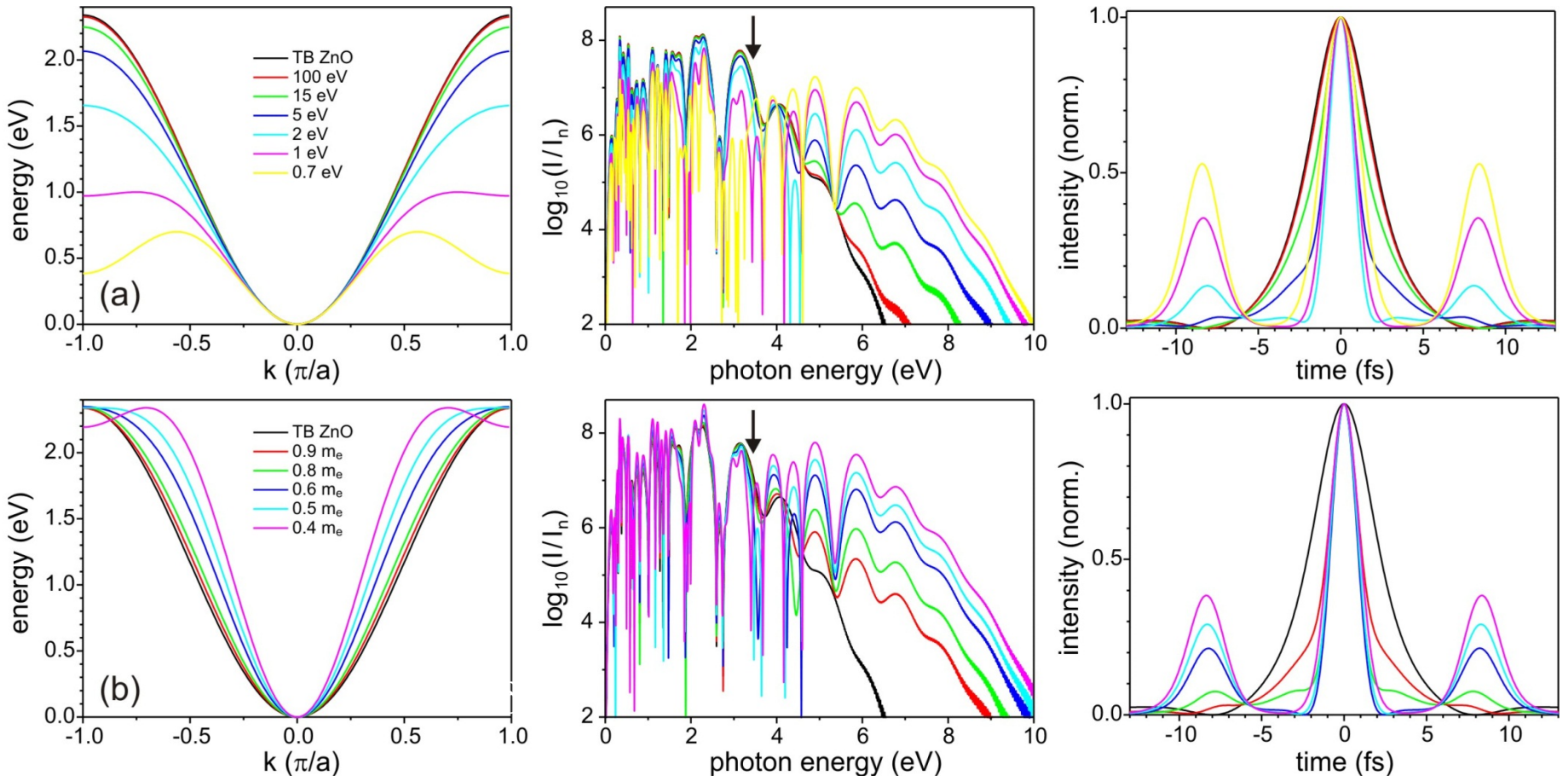

broadness of HHG emission is mainly determined by the maximum steepness of the band dispersion $\omega_e(k)$ since for a steeper dispersion the intraband acceleration leads to a faster variation of the electron energy via $k(t)$

Waveform-driven HHG from solids: intraband dynamics

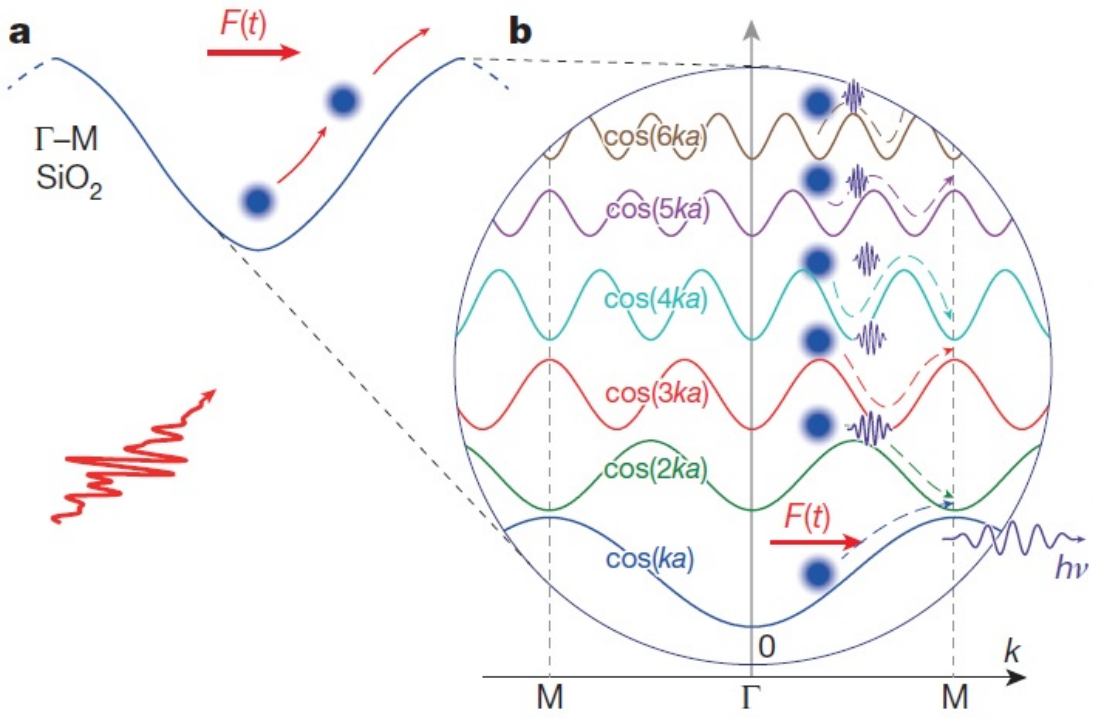

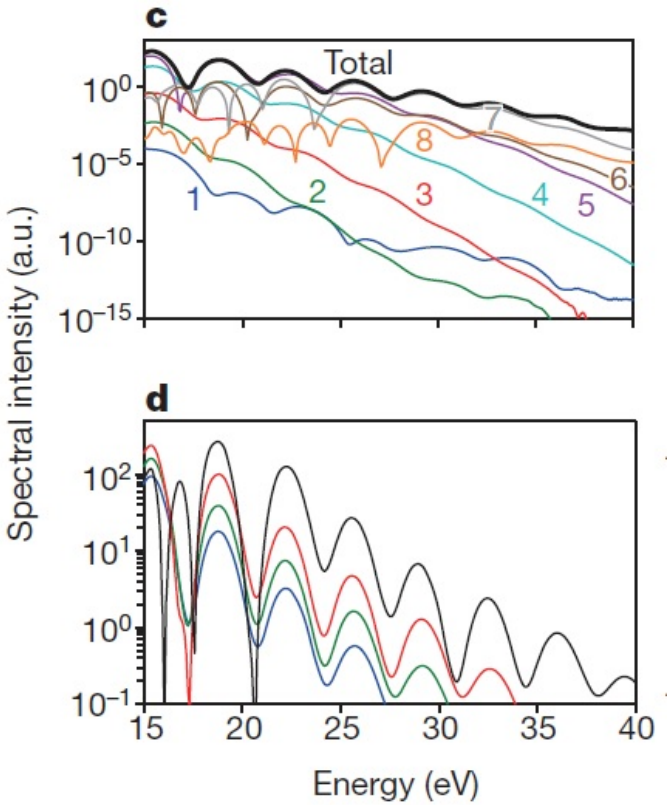

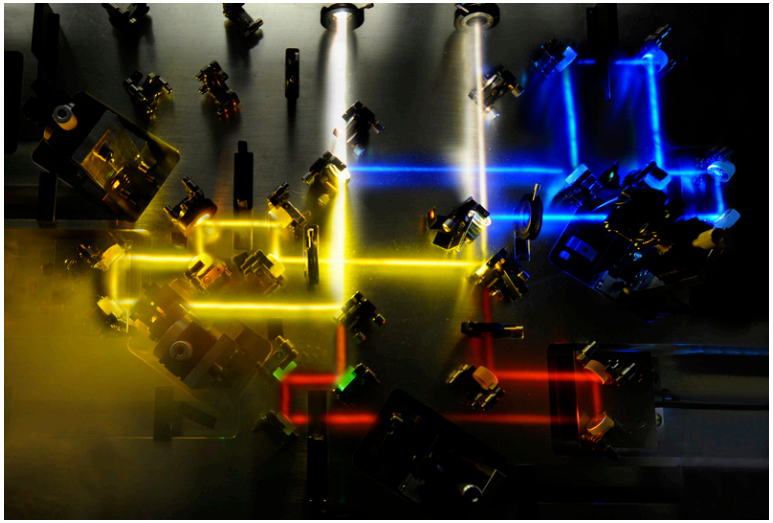

T. T. Luu *et al.*, Nature **521**, 498 (2015)
M. Garg *et al.*, Nature **538**, 359 (2016)

intraband dynamics (Bloch oscillations)

Waveform-driven HHG from solids: intraband dynamics

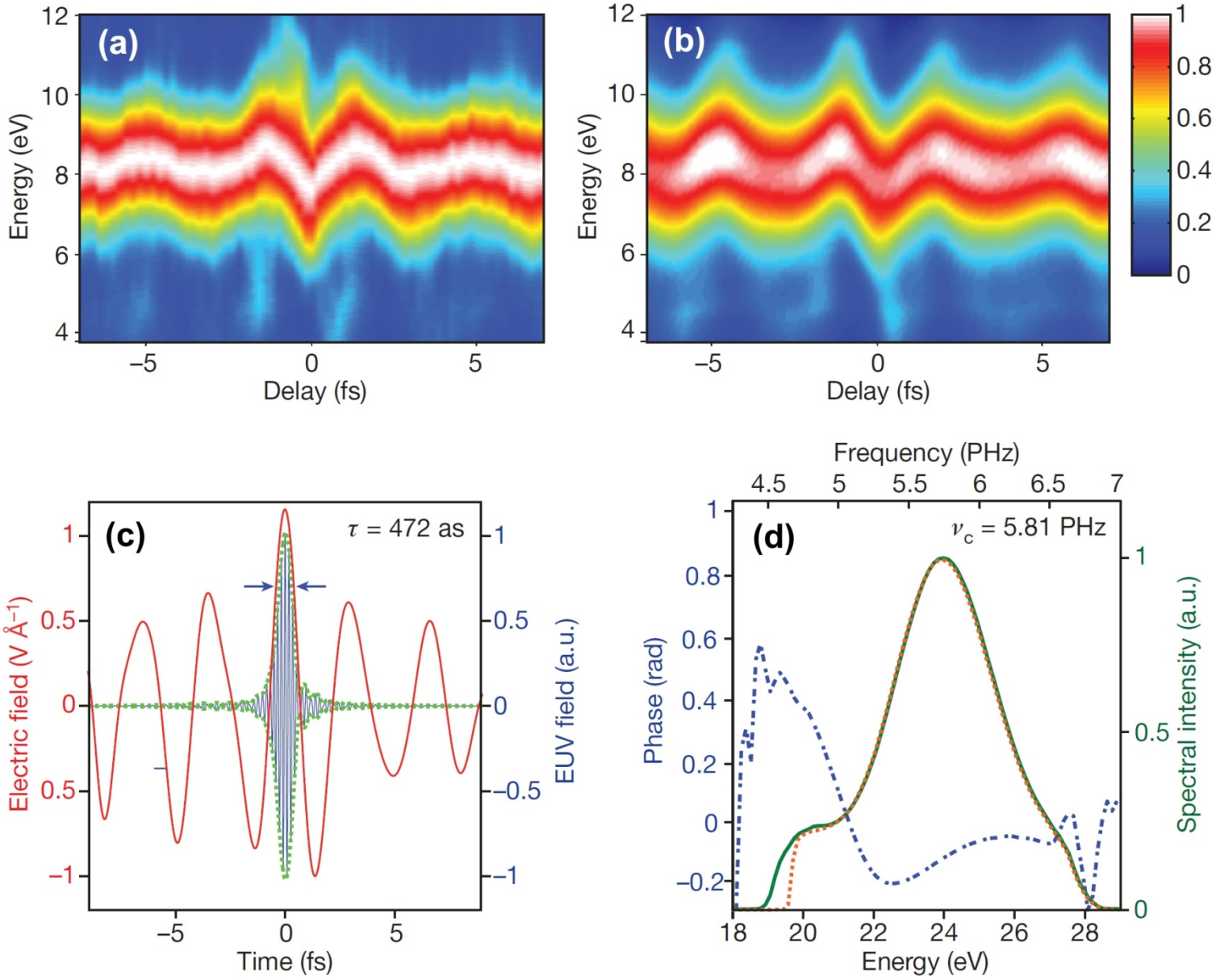

M. Garg *et al.*, Nature **538**, 359 (2016)

THz-driven HHG from solids: coupled intra-/interband dynamics

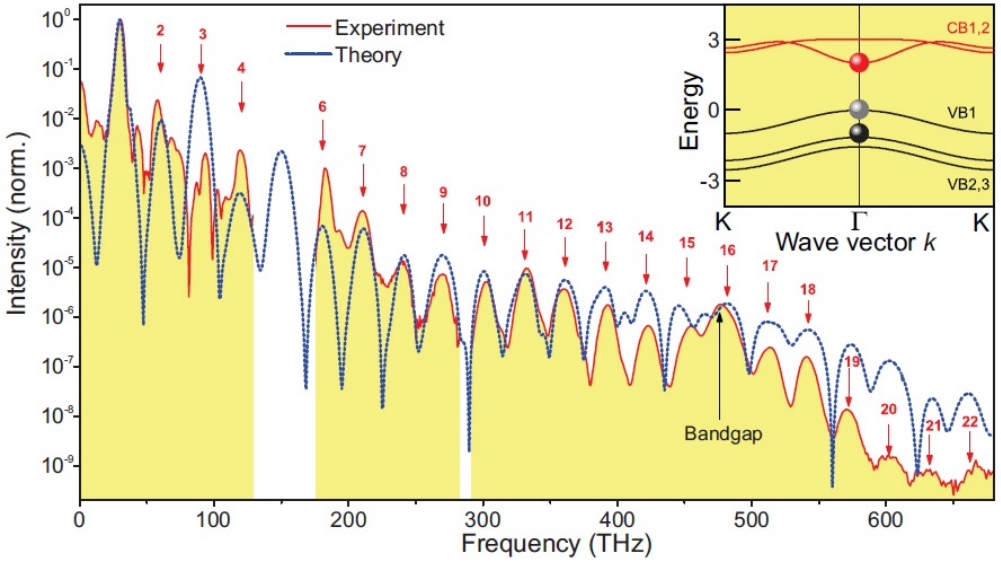

O. Schubert *et al.*,
Nature Phot. **8**, 119 (2014)

M. Hohenleutner *et al.*,
Nature **523**, 572 (2015)

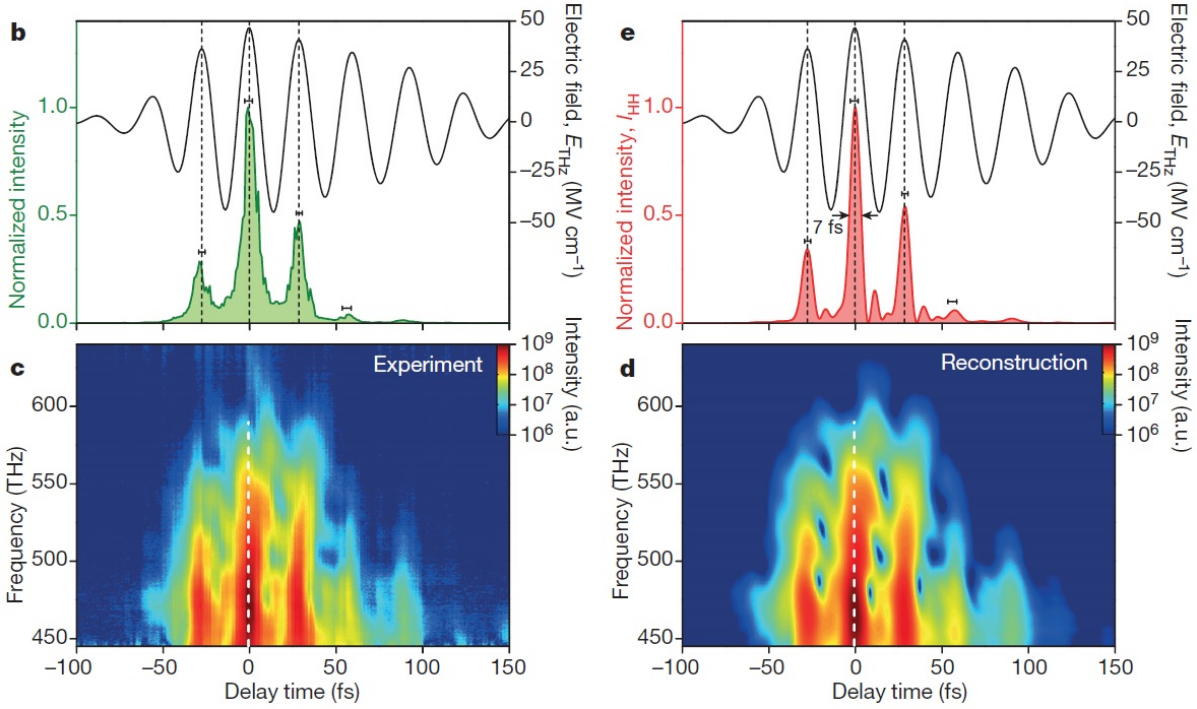

13.6.1 *Ab-initio* simulations based on time-dependent density-functional theory (TDDFT)

no *a priori* model assumptions, no strong approximations

full electronic structure (valence and conduction bands), real crystal structure

N. Tancogne-Dejean *et al.*, Phys. Rev. Lett in press (2017)

$$\mathrm{HHG}(\omega) \propto \left| \mathrm{FT}\left\{ \int_{\Omega} d^3\mathbf{r}\, n(\mathbf{r},t) \nabla v_0(\mathbf{r}) \right\} + N_e \mathbf{E}(\omega) \right|^2 . \qquad (13.56)$$

like HHG spectrum. The more interesting and relevant term for HHG is the first one in Eq. (13.56). It shows that higher harmonics are generated by two competing terms, the spatial variation of the total electronic density ($n(\mathbf{r},t)$) and the gradient of the electron-nuclei potential ($\nabla v_0(\mathbf{r})$), the latter being time independent, as ionic motion is neglected here. In gases, the gradient of the electron-nuclei potential is important, but the electronic density is low. In the case of solids, the electronic density is higher, but the potential is rather homogeneous, resulting in a smaller gradient of the potential than in the atomic case. In fact, in the limit of a homogeneous electron gas, the gradient becomes zero, and no harmonics are generated, irrespective of the value of the electronic density. In this case the bands are parabolic, thus we recover the known result that parabolic bands do not yield non-perturbative harmonics [69].

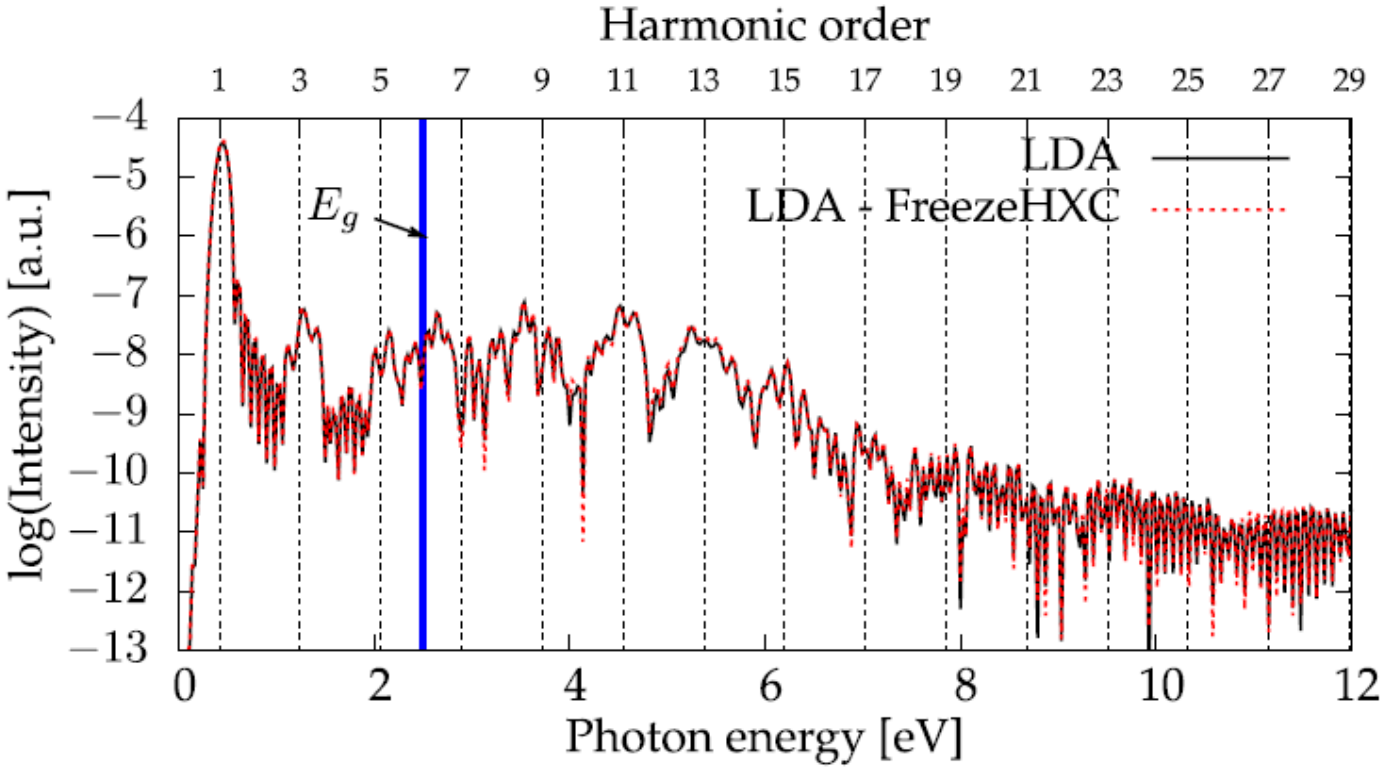

Figure 13.24: HHG spectra from bulk silicon, for polarization along $\overline{\Gamma X}$, computed within the LDA (LDA; black line) and within the LDA, but freezing the Coulomb and exchange-correlation terms to their ground-state value (LDA-FreezeHXC; red line). [83]

in silicon, electrons evolve mainly as independent particles in the ground-state potential → single-active electron (SAE) approximation good

might retrieve ground-state information (band structure) from HHG spectra

N. Tancogne-Dejean *et al.*, Phys. Rev. Lett **118**, 087403 (2017)

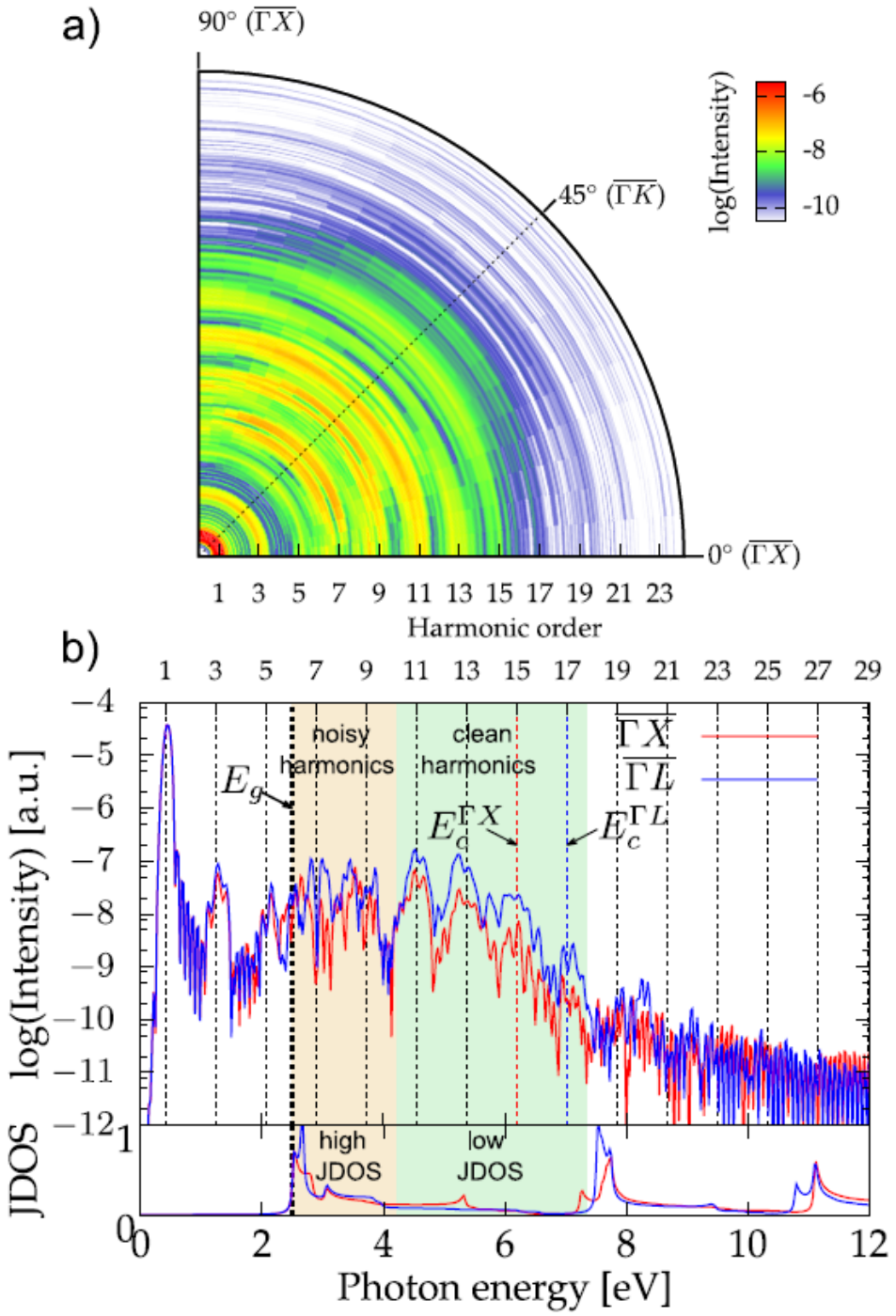

anisotrope HHG emission even for cubic crystal

joint density of state (JDOS)

low JDOS:
interband transitions suppressed
clean harmonics

N. Tancogne-Dejean *et al.*,
Phys. Rev. Lett **118**, 087403 (2017)

HHG cutoff independent of driver wavelength

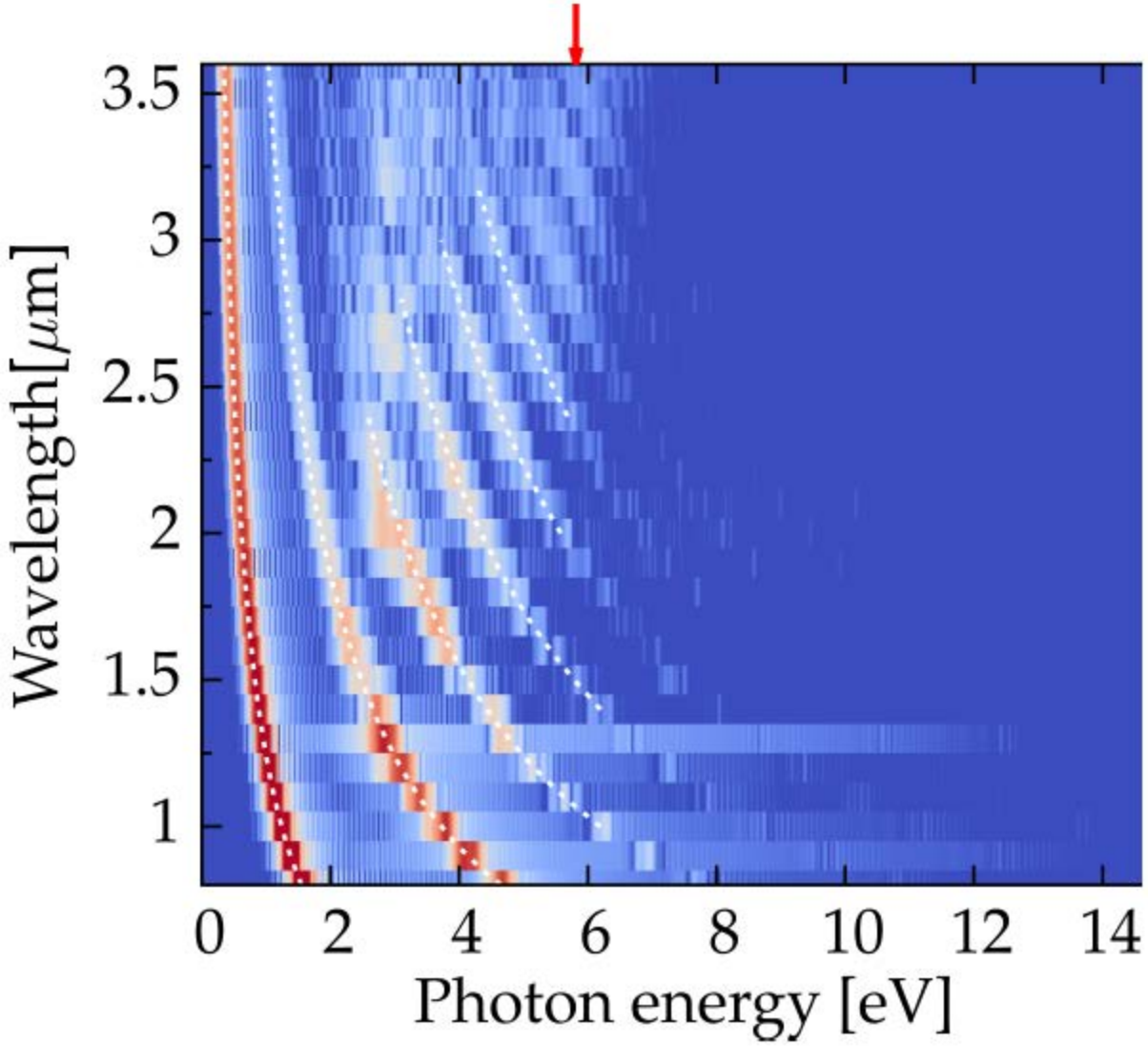

N. Tancogne-Dejean *et al.*, Phys. Rev. Lett **118**, 087403 (2017)

Summary of findings in Phys. Rev. Lett. 118, 087403 (2017)

To briefly summarize the findings by Tancogne-Dejean *et al.* [83]: it was shown analytically that HHG in solids is enhanced by the inhomogeneity of the electron-nuclei potential, and that the yield is increased for heavier atoms in the solid. The *ab-initio* TDDFT simulations demonstrated that HHG in bulk crystals is anisotropic, even in cubic materials. The simulations revealed that it is possible to suppress interband transitions in favor of HHG arising from intraband dynamics in solids, and most importantly to predict the optimal laser polarization, based on the sole knowledge of the crystal's band structure and its JDOS. Finally, the simulations confirmed without making any model assumptions that the cutoff of the HHG in solids is wavelength-independent. Further investigations should address extrinsic effects such as the electron-phonon coupling, propagation and surface effects. These findings and *ab-initio* TDDFT simulations can guide the search of better materials for solid-state high-harmonic sources and tailored HHG in solids.

polarization-state-resolved high-harmonic spectroscopy:

N. Klemke *et al.*, Nature Commun. **10**, 1319 (2019)

N. Tancogne-Dejean *et al.*, Nature Commun. **8**, 745 (2017)

Lightwave valleytronics in 2D transition metal dichalcogenides (2D TMDs)

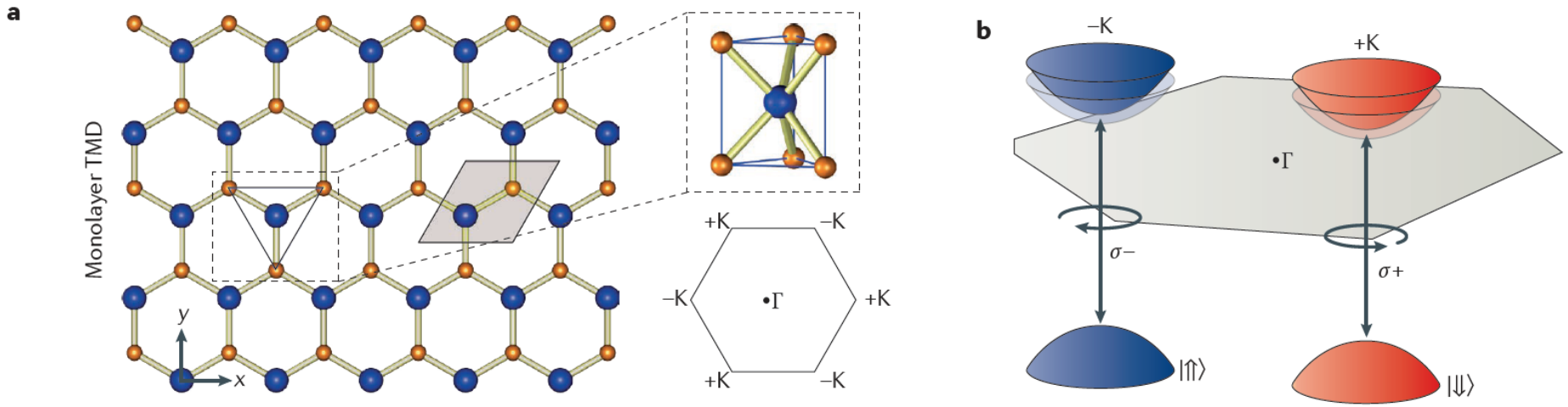

Figure 1 | **Valley-dependent carrier transport. a** | The 2D hexagonal crystal structure of a monolayer transition metal dichalcogenide (TMD) composed of transition metal atoms (blue) and chalcogen atoms (orange) resembles that of graphene but with broken inversion symmetry. A side view shows the 3D structure. The hexagonal Brillouin zone is shown labelling the Γ point and the two inequivalent +K and –K points. **b** | Valley-dependent optical selection rules for interband transitions in monolayer TMDs. σ+ polarized light couples to the +K (red) valley, and σ– polarized light couples to the –K (blue) valley. **c** | Illustration of the valley unpolarized electron and hole Hall effect, originating from the Berry-curvature

electrons in 2D crystals with a honeycomb lattice structure possess **valley pseudospin** degree of freedom, in addition to **charge** and **spin**
→ **valleytronics**

J. R. Schaibley *et al.*, Nature Reviews Materials **1**, 16055 (2016)

K. F. Mak and J. Shan, Nature Photonics **10**, 216 (2016)

HHG from strongly correlated materials: *ab-initio* TDDFT+*U* predictions for NiO

25 fs

3 μm (0.43 eV)

NiO

Nevill Francis Mott

Hubbard *U* decreases on sub-cycle time scale during the laser pulse

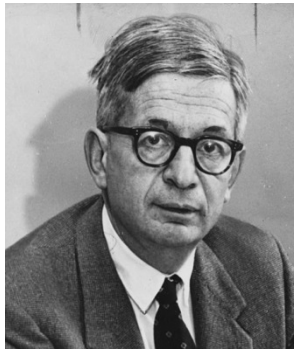

Rudolph Ernst Peierls

stronger laser pulses induce stronger and faster decrease of *U*

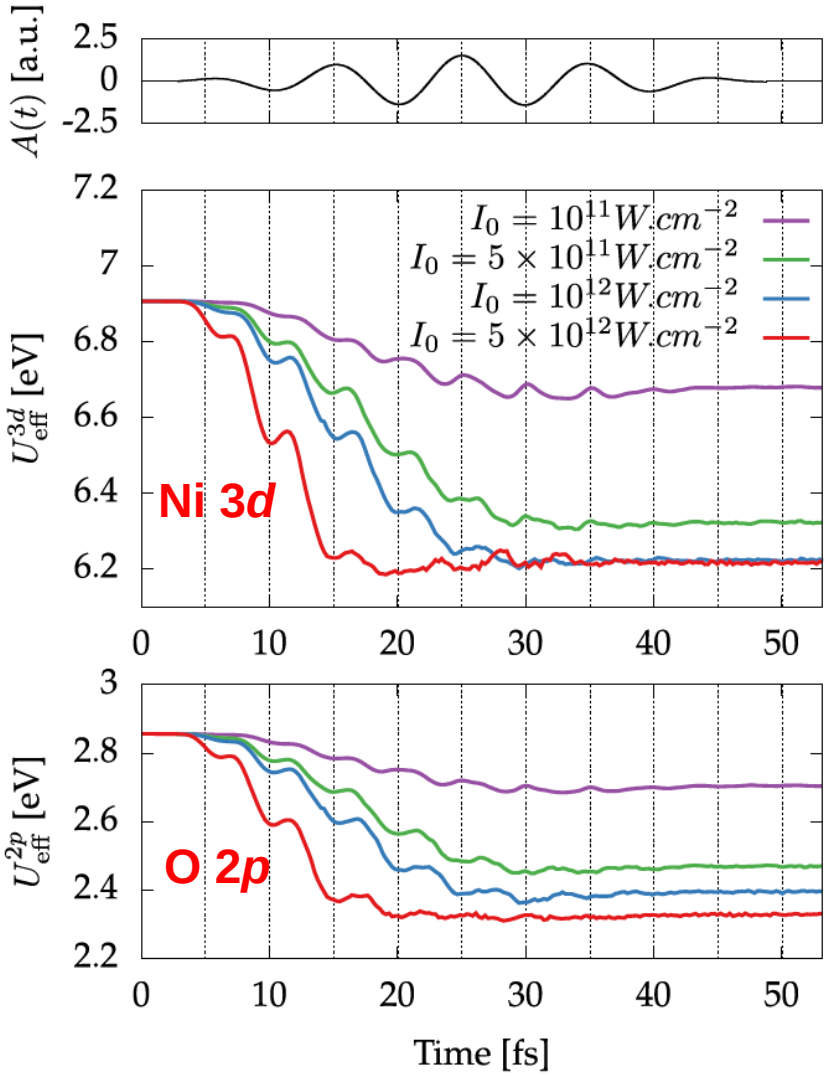

- N. Tanconge-Dejean, M. A. Sentef, and A. Rubio, Phys. Rev. Lett. **121**, 097402 (2018)
- TDDFT+*U*: N. Tancogne-Dejean, M. J. T. Oliveira, and A. Rubio, Phys. Rev. B **96**, 245133 (2017)
- N. F. Mott and R. Peierls, Proc. Phys. Soc. **49**, 72 (1937)

13.7 High-order sideband generation

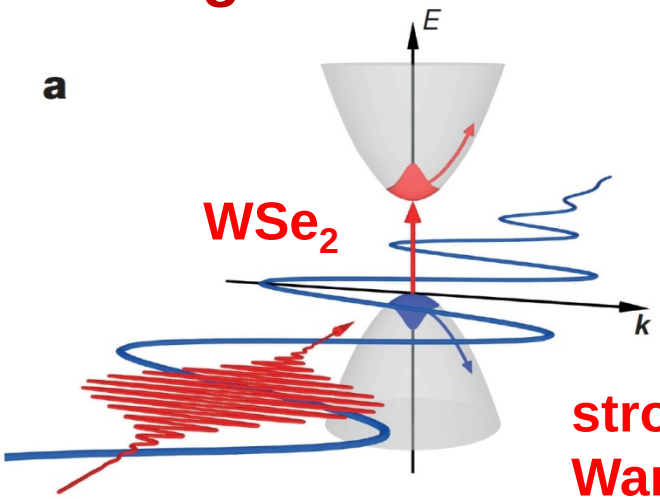

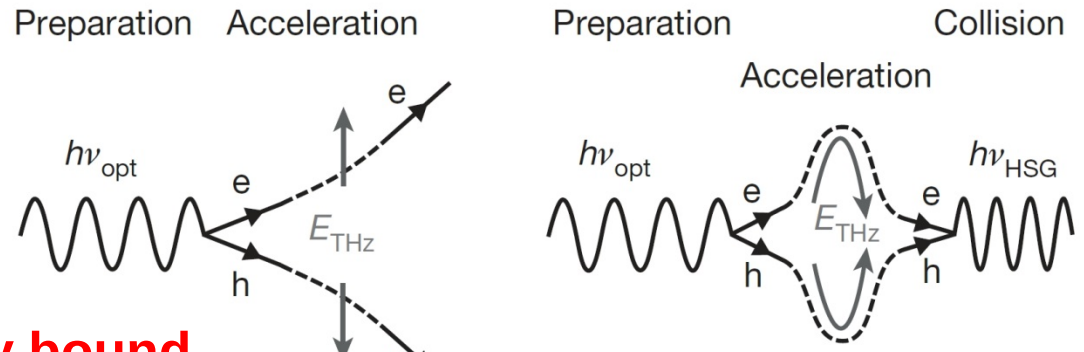

strongly bound Wannier exciton

lightwave-driven quasiparticle collider

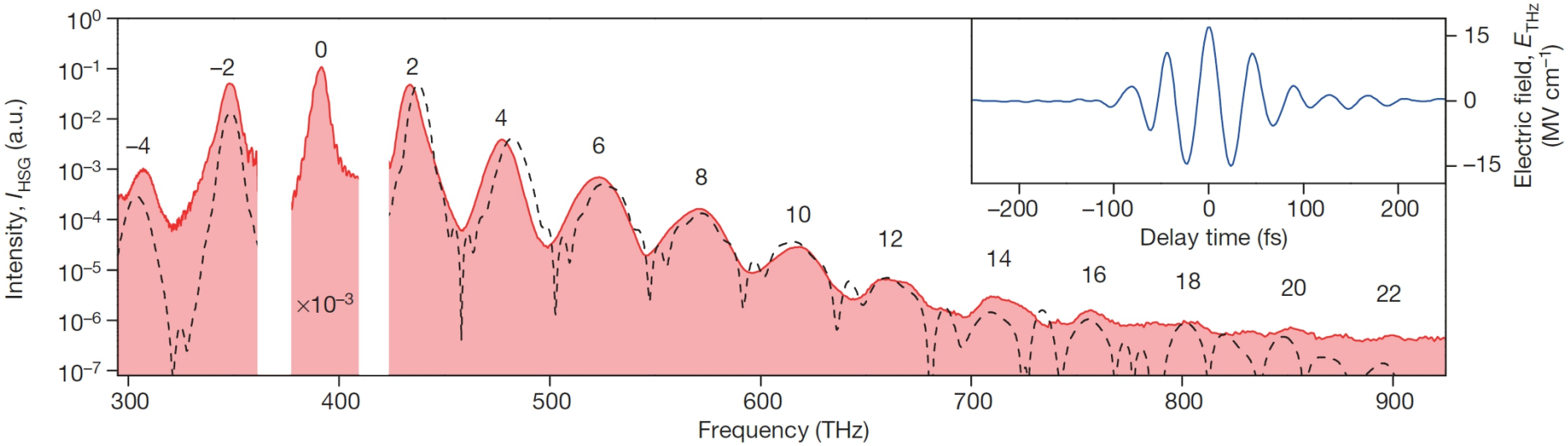

F. Langer *et al.*, Nature **533**, 225 (2016)

F. Langer *et al.*, Nature **557**, 76 (2018)

B. Zaks *et al.*, Nature **483**, 580 (2012) THz-FEL

13.8 Dynamical Franz-Keldysh effect

static Franz-Keldysh effect:
photon-assisted tunneling of electrons from valence to conduction band

dynamical Franz-Keldysh effect:
characterized by $U_p \approx \hbar\omega_0$, can be thought of as the point, where the **tunneling time is comparable to the light period** of the excitation field

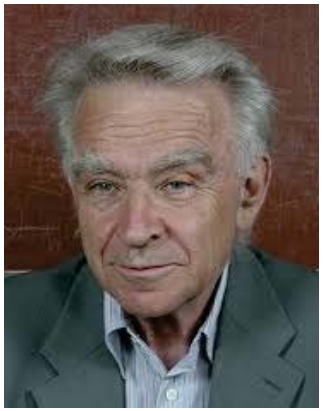

Walter Franz

Leonid V. Keldysh
annus mirabilis 1964

13.8 Dynamical Franz-Keldysh effect

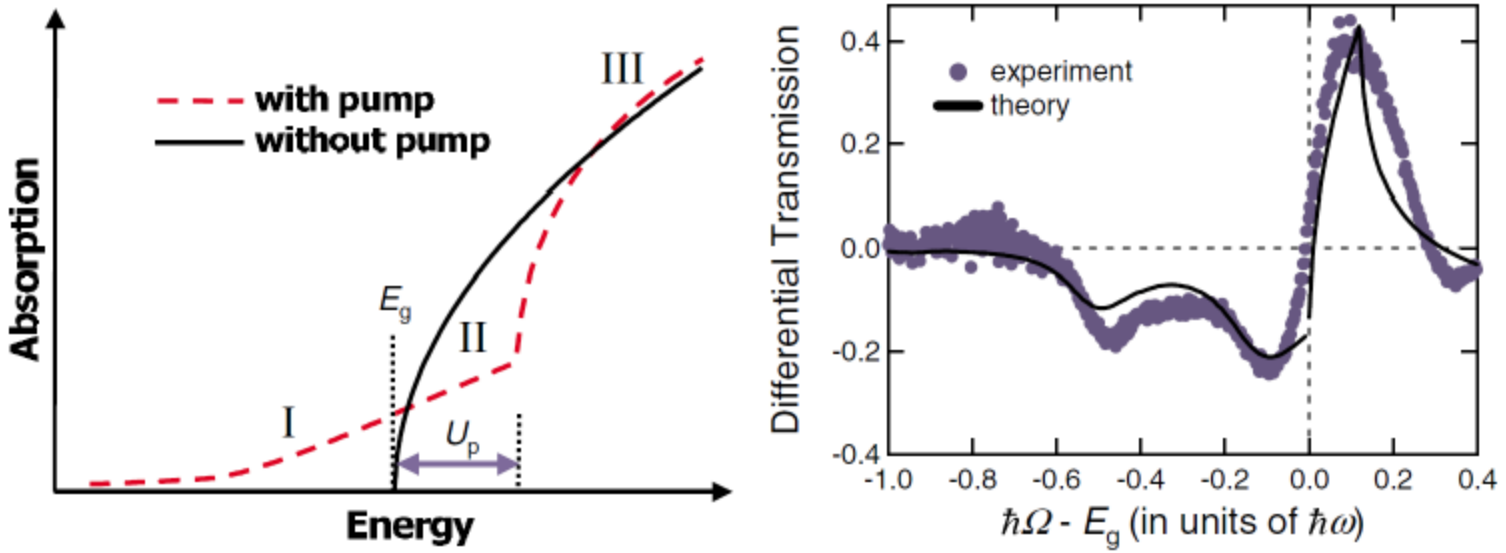

Figure 13.23: Dynamical Franz-Keldysh effect: (Left) Interband absorption in a direct-gap semiconductor near the band gap E_g without (solid line) and with (dashed line) a strong driving field. (Right) Experimental data in GaAs and fit by Yacoby's [24] theory. [77]

A. Srivastava *et al.*, Phys. Rev. Lett. **93**, 157401 (2004)

(i) induced below-band-gap absorption (region I),
(ii) blue shift (equal to U_p) of the band edge causing induced transparency (region II),
(iii) oscillatory behavior above the band gap (region III)

attosecond dynamical Franz-Keldysh effect in diamond

attosecond transient XUV absorption on polycrystalline diamond
5-fs IR pump, ~6.5×10^{12} W/cm^2
isolated 255-as XUV pulses (spectrum 35-50 eV)

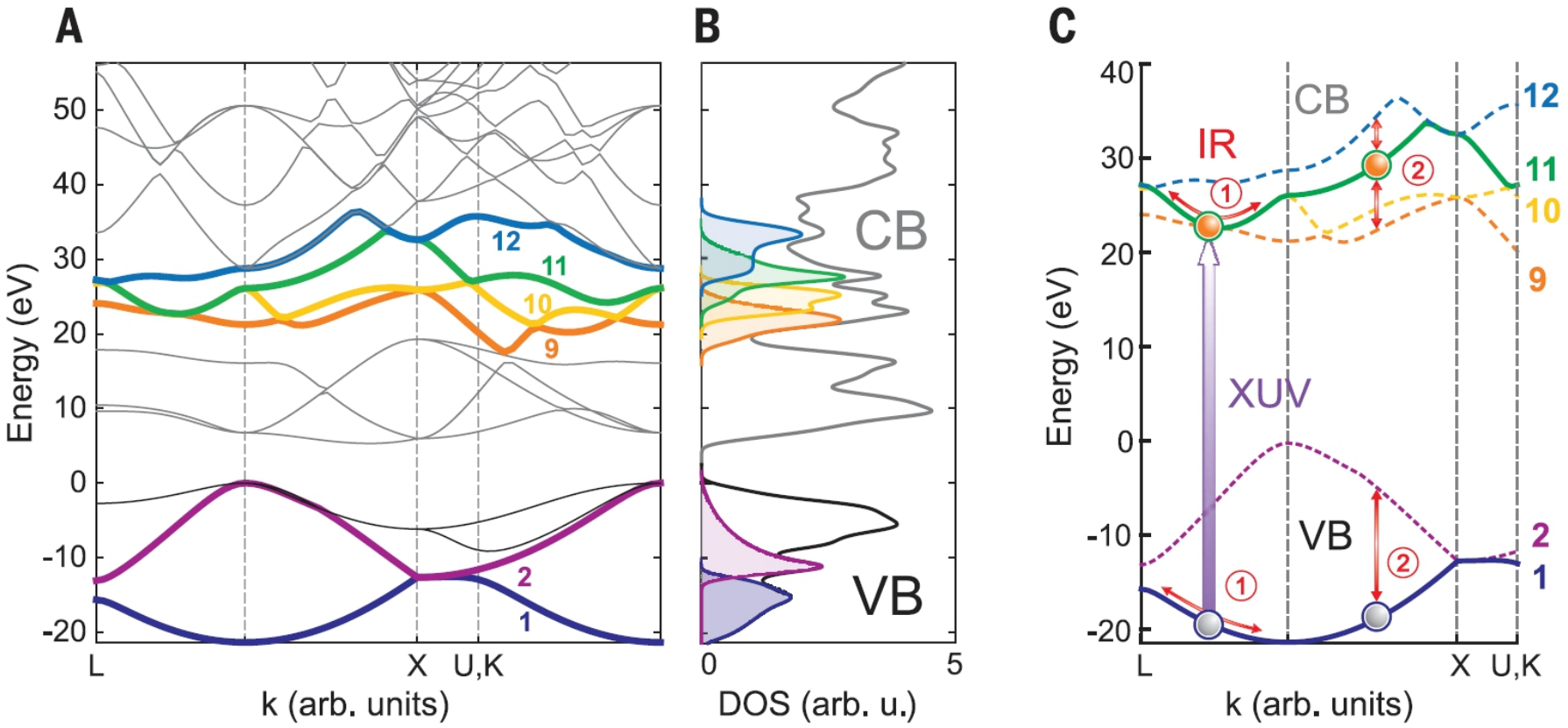

M. Lucchini *et al.*, Science **353**, 916 (2016)

attosecond dynamical Franz-Keldysh effect in diamond

attosecond transient XUV absorption on polycrystalline diamond
5-fs IR pump, ~6.5×10^{12} W/cm^2
isolated 255-as XUV pulses (spectrum 35-50 eV)

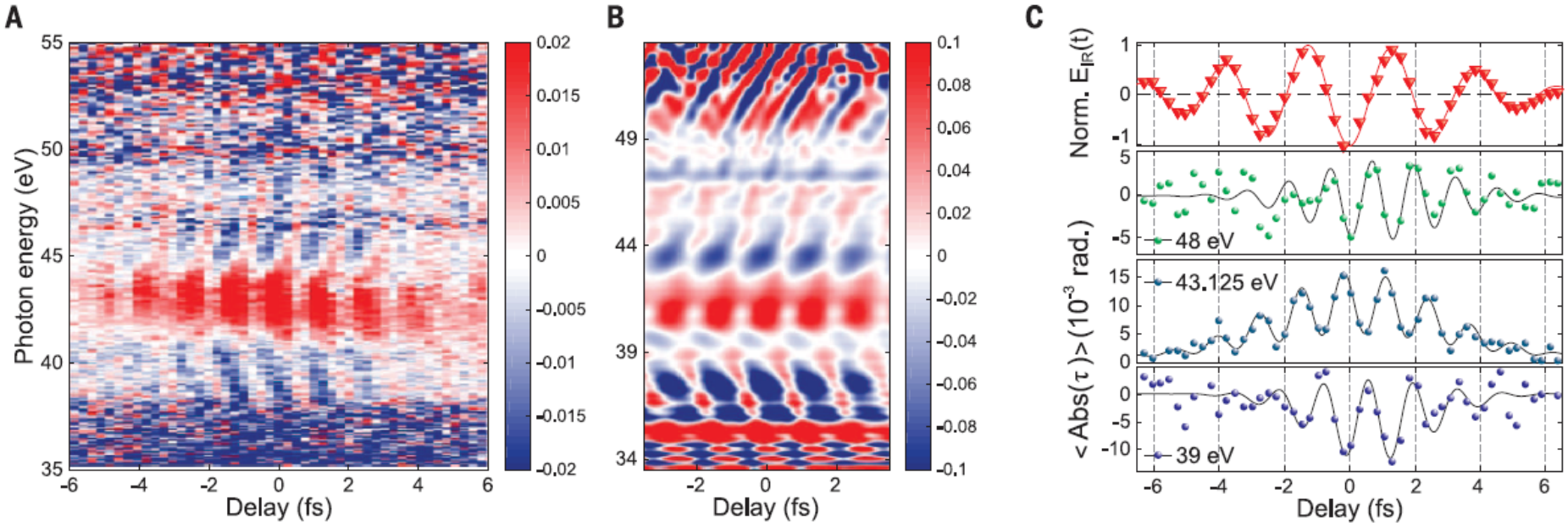

$$\Delta \mathrm{Abs}(E_{\mathrm{ph}}, \tau) = \Delta\alpha(E_{\mathrm{ph}}, \tau)L = (\alpha_{\mathrm{IR}}(E_{\mathrm{ph}}, \tau) - \alpha_0(E_{\mathrm{ph}}))L = \ln\left(\frac{I_{\mathrm{t}}(E_{\mathrm{ph}})}{I_{\mathrm{t}}^{\mathrm{IR}}(E_{\mathrm{ph}}, \tau)}\right). \quad (13.57)$$

IR-pump-induced changes oscillate at $2\omega_{IR}$

M. Lucchini *et al.*, Science **353**, 916 (2016)